www.lpr-journal.org

LASER & PHOTONICS REVIEWS

WILEY-VCH

Abstract Whispering-gallery modes (WGM) on a spherical surface were first described by Lord Rayleigh at the beginning of the last century, but only after the invention of laser did they start to have some scientific relevance and only during the last two decades there has been a substantial move towards real devices and practical applications. WGM resonators have peculiar properties, the most notable being the potential of having an ultrahigh quality factor Q, which makes them very appealing both as laser cavities and as extremely sensitive sensors. Among the different types of WGM resonators, the microspherical ones represent a very important category, due to their simplicity, easy fabrication, and very high quality. In this review we provide a description of their fundamental properties and we summarize recent works on their application as filters, sensors and lasers.

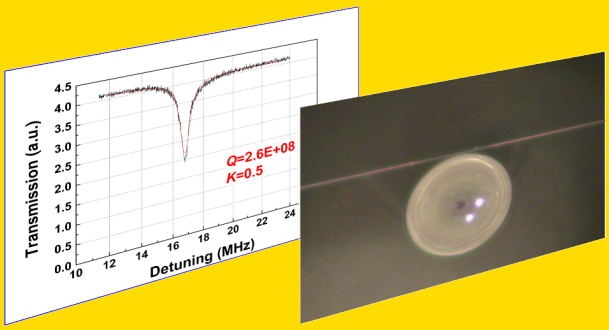

Spherical whispering-gallery-mode microresonators

Alessandro Chiasera[1], *Yannick Dumeige*[2], *Patrice Féron*[2], *Maurizio Ferrari*[1], *Yoann Jestin*[1], *Gualtiero Nunzi Conti*[3,4], *Stefano Pelli*[4], *Silvia Soria*[3,4], *and Giancarlo C. Righini*[4,*]

[1] CSMFO Lab, Istituto di Fotonica e Nanotecnologie (IFN-CNR), Via alla Cascata 56/C, 38050 Povo-Trento, Italy
[2] ENSSAT-FOTON (CNRS-UMR 6082), ENSSAT-Université de Rennes 1, 6 rue de Kerampont, BP 80518, 22300 Lannion, France
[3] Centro Studi e Ricerche "E. Fermi", Piazza del Viminale 2, 00184 Rome, Italy
[4] MDF Lab, "Nello Carrara" Institute of Applied Physics (IFAC-CNR), Via Madonna del Piano 10, 50019 Sesto Fiorentino, Firenze, Italy

Received: 25 February 2009, Revised: 24 April 2009, Accepted: 18 May 2009
Published online: 13 July 2009

Key words: Resonators, WGM, microcavity laser, biosensor, glass.

PACS: 42.25.Bs, 42.55.Sa, 42.60.Da, 42.70.Ce, 42.82.Et, 87.85.fk

1. Introduction

A set of two or more mirrors arranged to keep light propagating in a closed path constitutes what is generally called an optical cavity or an optical resonator. Interactions of light with matter are greatly enhanced in high-quality optical resonators, which are able to confine significant optical powers in small spaces for extended time periods [1–4]. These structures have therefore always attracted considerable scientific and technological interest due to their potential applications in nonlinear optics, optical signal processing, and sensing. Even if a primary area is that of laser resonators [5–9], one could easily assert that optical resonators play a ubiquitous role in modern optics. Fabrication of good optical mirrors, their alignment, and binding, however, represent a rather difficult and expensive task.

A particular class of optical resonators, which overcome the assembling problem, is constituted by spherical dielectric structures, where optical rays are totally internally reflected and focused by the surface itself. A nonabsorbing dielectric sphere can sustain whispering-gallery modes (WGMs), that can be interpreted as electromagnetic waves that circulate and are strongly confined within the sphere. Due to minimal reflection losses and to potentially very low material absorption, these modes can reach exceptionally high quality factors (Q).

WGMs were first observed in the dome of St Paul's Cathedral in London, designed by the famous architect and scientist Sir Christopher Wren (who, by the way, was one of the founder members of the "Royal Society of London for the Improvement of Natural Knowledge", known simply as the *Royal Society*). One gallery, 32 m in diameter, runs around the interior of the dome at about 30 m above

* Corresponding author: e-mail: giancarlo.righini@cnr.it, g.c.righini@ifac.cnr.it

the cathedral floor, and can be reached by 259 steps from ground level. It got the name of *Whispering Gallery* because a whisper against its wall at any point is audible to a listener with an ear held to the wall at any other point around the gallery. It was two centuries after the completion of the cathedral, officially set on 1711, that John William Strutt (Lord Rayleigh) identified the refocusing effect of the curved surface as the sound travels along the gallery, and in the years 1910–1912 published *The Problem of the Whispering Gallery* [10]; he also suggested that such modes of the electromagnetic field could find some practical applications due to the extreme confinement of the field. It may be interesting to recall that this problem attracted the attention of Sir C. V. Raman as well, who carried out some observations in St. Paul's Cathedral and also in a semicircular archway at the University College Laboratory, and reported them to the Royal Society [11].

Whispering-gallery modes (sometimes also referred to as MDR's, morphology-dependent resonances [12, 13]) have since then been studied at sound, optical and microwave wavelengths in various systems, including cylindrical geometries, micrometer-sized liquid droplets, and glass and crystal spheres. A pioneering approach to the study of the resonances in a suitably shaped object made of a dielectric material was published by Richtmyer in 1939 [14]; he showed that a spherical microparticle could sustain high-Q resonance modes. Garrett et al., in 1961, first noticed that spherical resonators for optical waves could be used as laser resonators; they observed pulse laser oscillation in highly polished Sm^{+2}-doped CaF_2 spheres with diameter between one and two mm [15].

More recently, WGM resonators have attracted increasing attention [16–18], especially in view of the great potential in the areas of optical communications signal processing and biochemical sensing. Various geometries have been explored, like micropillars [19], microrings [20–23], microdisks [24–27], microtoroids [28–31], photonic-crystal cavities [32–34]. The goals of circuit integration and cost-saving mass-manufacturing processes have addressed much of the research towards planar geometries: waveguide-based structures like rings and disks, which can be microfabricated onto wafer substrates using conventional integrated-circuit deposition and etching techniques, have been demonstrated as channel-dropping filters, switches, and even add-drop multiplexers [17, 21–23].

The microspheres are the simplest three-dimensional WGM resonators, typically ten to a hundred micrometers in diameter, often fabricated in silica glass by simply melting the tip of an optical fiber. Despite the ease of fabrication, the resonance structure of a microsphere differs considerably from that of a planar waveguide ring resonator. Indeed, a spherical cavity can support very complicated modes with equatorial, radial, as well as polar field dependencies. The total optical loss in such resonators can be extremely low, and the resulting extraordinary high Q values of 10^8–10^9 lead to high energy density, narrow resonant-wavelength lines and a lengthy cavity ringdown. Liquid microspheres can also be considered, and indeed early experiments studied WGMs and laser emission in liquid microdroplets flying in air [35–39]. Tzeng et al., for instance, introduced a new optical technique, based on morphology-dependent peaks in the fluorescence spectra, to determine the evaporation and condensation rates of a linear stream of ethanol droplets impregnated with fluorescent dye molecules [35]. On irradiation of the droplets with a single N_2 laser pulse, the evaporation and condensation rates were deduced from the wavelength shift (to the blue or to the red, respectively) of the spectrally narrow structure-resonance peaks in the fluorescence spectra. The same authors observed laser action from individual ethanol droplets (60-μm diameter) containing Rhodamine 6G dye and pumped by a cw laser at 514.5 nm; laser emission was at wavelengths corresponding to the morphology-dependent resonances of a spherical droplet [36].

Micrometer-sized droplets of Rh-6G solution in water and ethanol were also investigated by Biswas et al. [38], who irradiated the droplets by high-intensity nanosecond pulses from a frequency-doubled Nd:YAG laser. Coupling of the spontaneous fluorescence emission with natural resonant modes of the spherical droplets resulted in stimulated emission, with each droplet behaving like a laser cavity with a Q value of the order of 7×10^4. They observed that emission exhibited faster rise times and was shorter lived than corresponding bulk-liquid fluorescence; it was also concluded that lasing in droplets is generally initiated almost simultaneously with elastic scattering, unlike stimulated Raman scattering, which is significantly delayed.

The effects of WGMs on radiative emission rates and on dipole-dipole energy transfer rates between molecules embedded in aerosol droplets were studied by developing a theory based on electromagnetic solutions for a dielectric sphere [39]. A later paper reported the effects of spatial hole burning on lasing of droplets (15.3 μm diameter) constituted by Rh-6G water solution [40]. Several mode orders, each forming a cluster of four to six WGM's were observed lasing simultaneously, the lowest-mode-order clusters being red-shifted in wavelength with respect to higher orders. The relative intensities of the modes were explained by using an output coupling theory that considered the gain enhancement resulting from cavity quantum electrodynamics (QED) effects and mode Qs calculated from Lorenz-Mie theory. In this case an upper limit of 10^8 for the Q of a nondegenerate cavity mode was estimated from the experimental data.

In the present paper, after reviewing the basic concepts of WGM propagation, we will focus on fabrication, characterization and application of solid microspheres, mostly produced in silica or multicomponent glasses. The challenge of efficiently accessing a high-Q microresonator, namely coupling light in and out, will also be discussed.

2. Physical basis of spherical microresonators

In the optical domain, whispering-gallery modes can be viewed as high angular momentum electromagnetic modes

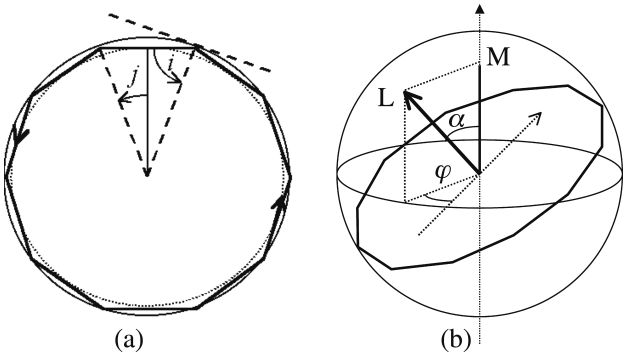

Figure 1 (a) Ray of light propagation by TIR. Definition of complementary angles i and j. (b) Angular momentum L associated to a WGM and its M projection on polar axis.

in which light propagates by repeated total internal reflections (TIR) with the proper phase condition after circling along the sphere surface. Let us consider a microsphere of radius a with refractive index N and a ray of light propagating inside, hitting the surface with angle of incidence i (Fig. 1a). If $i > i_c = \arcsin(1/N)$, then total internal reflection occurs. Because of spherical symmetry, all subsequent angles of incidence are the same, and the ray is trapped. This simple geometric picture leads to the concept of resonances. For large microspheres ($a \gg \lambda$), the trapped ray propagates close to the surface, and traverses a distance $\approx 2\pi a$ in a round trip. If one round trip exactly equals ℓ wavelengths in the medium ($\ell =$ integer), then one expects a standing wave to occur. This condition translates into $2\pi a \approx \ell(\lambda/N)$ since λ/N is the wavelength in the medium. In terms of the size parameter the resonance condition is $x = 2\pi a/\lambda \approx \ell/N$. The number of wavelengths ℓ in the circumference can be identified as the angular momentum in the usual sense. Indeed, let us consider the ray in Fig. 1a as a photon. Its momentum is $p = \hbar k = \hbar 2\pi N/\lambda$ where k is the wave number. If this ray strikes the surface at near-glancing incidence ($i \approx \pi/2$), then the angular momentum, denoted as L, is $L \approx ap = a2\pi\hbar N/\lambda = \hbar\ell$. For lower incidences, one expects other resonances at very close frequencies, characterized by the radius of the caustic $r_1 = a\cos j$ under the condition $a/N < r_1 < a$.

2.1. The electromagnetic problem

To solve the electromagnetic problem we use the so-called Hansen's method [41] where solutions of the vectorial Helmholtz equation have an angular dependence described by vectorial spherical harmonics [42] defined as:

$$\begin{cases} \mathbf{Y}_{\ell m}^{(\mathrm{m})} = \boldsymbol{\nabla} Y_\ell^{\mathrm{m}} \times \mathbf{r}/\sqrt{\ell(\ell+1)} & \text{denoted} \quad \mathbf{X}_\ell^{\mathrm{m}} \\ \mathbf{Y}_{\ell m}^{(\mathrm{e})} = r\boldsymbol{\nabla} Y_\ell^{\mathrm{m}}/\sqrt{\ell(\ell+1)} & \text{denoted} \quad \mathbf{Y}_\ell^{\mathrm{m}} \\ \mathbf{Y}_{\ell m}^{(E} = Y_\ell^{\mathrm{m}}\hat{r} & \text{denoted} \quad \mathbf{Z}_\ell^{\mathrm{m}} \end{cases}, \tag{1}$$

where superscripts (m) and (e) correspond to the magnetical or electrical character of the radiated field by the ℓ order multipole. They are associated to TE and TM modes, respectively. Superscript (o) corresponds to the radial character of the corresponding field. Formally, we can express the fields for both polarizations:

$$\begin{cases} \mathbf{E}_{\ell m}^{\mathrm{TE}}(\mathbf{r}) = E_{\mathrm{o}} \dfrac{f_\ell(r)}{k_{\mathrm{o}} r} \mathbf{X}_\ell^{\mathrm{m}}(\theta,\varphi)\,, \\ \mathbf{B}_{\ell m}^{\mathrm{TE}}(\mathbf{r}) = \dfrac{E_{\mathrm{o}}}{ic}\left(\dfrac{f'_\ell(r)}{k_{\mathrm{o}}^2 r} \mathbf{Y}_\ell^{\mathrm{m}}(\theta,\varphi) + \sqrt{\ell(\ell+1)} \dfrac{f_\ell(r)}{k_{\mathrm{o}}^2 r^2} \mathbf{Z}_\ell^{\mathrm{m}}(\theta,\varphi) \right), \end{cases} \tag{2}$$

$$\begin{cases} \mathbf{E}_{\ell m}^{\mathrm{TM}}(\mathbf{r}) = \dfrac{E_{\mathrm{o}}}{N^2}\left(\dfrac{f'_\ell(r)}{k_{\mathrm{o}}^2 r} \mathbf{Y}_\ell^{\mathrm{m}}(\theta,\varphi) + \sqrt{\ell(\ell+1)} \dfrac{f_\ell(r)}{k_{\mathrm{o}}^2 r^2} \mathbf{Z}_\ell^{\mathrm{m}}(\theta,\varphi) \right), \\ \mathbf{B}_{\ell m}^{\mathrm{TM}}(\mathbf{r}) = -\dfrac{iE_{\mathrm{o}}}{c} \dfrac{f_\ell(r)}{k_{\mathrm{o}} r} \mathbf{X}_\ell^{\mathrm{m}}(\theta,\varphi)\,, \end{cases} \tag{3}$$

where $f_\ell(r) = \psi_\ell(Nk_{\mathrm{o}}r)$ for $r < a$ and $f_\ell(r) = \alpha\psi_\ell(k_{\mathrm{o}}r) + \beta\chi_\ell(k_{\mathrm{o}}r)$ for $r > a$ are solutions of a Riccati-Bessel radial equation, and $\psi_\ell(\rho) = \rho j_\ell(\rho)$ and $\chi_\ell(\rho) = \rho n_\ell(\rho)$, where j_ℓ and n_ℓ are spherical Bessel and Neumann functions, respectively.

2.2. Positions of resonances

The condition of continuity of tangential components of the fields allows us to find equations for the positions of resonances,

$$\begin{cases} \psi_\ell(Nk_0a) = \alpha\psi_\ell(k_0a) + \beta\chi_\ell(k_0a) \\ P\psi'_\ell(Nk_0a) = \alpha\psi'_\ell(k_0a) + \beta\chi'_\ell(k_0a) \end{cases}, \tag{4}$$

where $P = N$ for TE polarization ($P = N^{-1}$ for TM). The exact solutions go through determination of constants α and β and lead to complex frequencies. As a first approximation we assume the radiative part outside the sphere is negligible. The resonance condition expressed in size parameter $x = 2\pi a/\lambda$ can be written as:

$$P\frac{\psi'_\ell(Nx)}{\psi_\ell(Nx)} = \frac{\chi'_\ell(x)}{\chi_\ell(x)}\,, \tag{5}$$

and translating the spherical Bessel and Neumann functions to their cylindrical counterparts we obtain:

$$P\frac{J'_\nu(Nx)}{J_\nu(Nx)} = \frac{N'_\nu(x)}{N_\nu(x)} \tag{6}$$

where $\nu = \ell + 1/2$.

Even under this approximated equation, the solutions x have to be numerically evaluated. In order to obtain analytical expressions for the positions of resonances we use the method developed by Lam et al. [43]. ν, which corresponds classically to the angular momentum, is such that $\nu = Nx\sin i$ and due to the total internal reflection we have $x \leqslant \nu \leqslant Nx$. Thus, when $x \gg 1$, ν and x are of the same order (i.e. $\mu = \nu/x \approx 1$). Moreover, for well confined WGMs, the angle $i \approx \pi/2$ and one expects a very low value for the quantity $|Nx - \nu|$. Introducing $t = O(1)$, this quantity is such that:

$$Nx = \nu + t\nu^{1/3}\,. \tag{7}$$

The Bessel and Neumann functions $J_\nu(Nx)$ and $N_\nu(x)$ in Eq. (6) can be expressed as asymptotic series in powers of $\nu^{-1/3}$ [44]:

$$J_\nu(Nx) \approx \frac{2^{1/3}}{\nu^{1/3}}\,\mathrm{Ai}(-2^{1/3}t)\left[1+\sum_{j=1}^{\infty} f_j(t)/\nu^{2j/3}\right] + \frac{2^{2/3}}{\nu}\,\mathrm{Ai}'(-2^{1/3t})\sum_{j=0}^{\infty} g_j(t)/\nu^{2j/3} \tag{8}$$

$$N_\nu(x) \approx -\frac{\mathrm{e}^{\nu(\beta-\tanh\beta)}}{\sqrt{\pi\nu(\tanh\beta)/2}} \times\left[1+\sum_{j=1}^{\infty}(-1)^j\frac{u_j(\coth\beta)}{\nu^j}\right], \tag{9}$$

and for their derivatives:

$$J'_\nu(Nx) \approx \frac{2^{2/3}}{\nu^{2/3}}\,\mathrm{Ai}'(-2^{1/3t})\left[1+\sum_{j=1}^{\infty} h_j(t)/\nu^{2j/3}\right] + \frac{2^{1/3}}{\nu^{4/3}}\,\mathrm{Ai}(-2^{1/3t})\sum_{j=0}^{\infty} l_j(t)/\nu^{2j/3} \tag{10}$$

$$N'_\nu(x) \approx \sqrt{\frac{\sinh 2\beta}{\pi\nu}}\,\mathrm{e}^{\nu(\beta-\tanh\beta)} \left[1+\sum_{j=1}^{\infty}(-1)^j\frac{u_j(\coth\beta)}{\nu^j}\right]. \tag{11}$$

In these expressions, Ai is the Airy function, f_j, g_j, h_j, l_j, and u_j are polynomials [44] and $\cosh\beta = \mu$.

To first order, each part of Eq. (6) can be written as:

$$P\frac{J'_\nu(Nx)}{J_\nu(Nx)} \approx -P\frac{2^{1/3}}{\nu^{1/3}}\frac{\mathrm{Ai}'(-2^{1/3}t)}{\mathrm{Ai}(-2^{1/3}t)}\,, \tag{12}$$

$$\frac{N'_\nu(x)}{N_\nu(x)} \approx -|\sinh\beta| = -\sqrt{\mu^2-1}\,. \tag{13}$$

In Eqs. (12) and (13), when $\nu \to \infty$ the power $1/3$ of ν can be compensated only if $\mathrm{Ai}(-2^{1/3}t) = O(\nu^{-1/3})$. Consequently, $2^{1/3}t$ must be close to a root α_n of $\mathrm{Ai}(-z)$:

$$2^{1/3}t = \alpha_n + O(\nu^{-1/3}). \tag{14}$$

Thus, introducing this result in Eq. (7) we obtain for the resonance positions to first order:

$$Nx_{\ell,n} = \nu + 2^{-1/3}\alpha_n\nu^{1/3} + O(1), \tag{15}$$

with $\nu = \ell + \frac{1}{2}$. At higher order we obtain:

$$Nx_{\ell,n} = \nu + a_{1n}\nu^{1/3} + a_0\nu^0 + a_{-1n}\nu^{-1/3} + \cdots, \tag{16}$$

with $a_{1n} = 2^{-1/3}\alpha_n$, $a_0 = -\frac{P}{\sqrt{N^2-1}}$ and $a_{-1n} = \frac{3}{10}2^{-2/3}\alpha_n^2$.

For a given polarization (TE or TM), three integers n, ℓ, m characterize the resonances. The order n of the root α_n of the Airy function is associated with the radial function and the classical quantization for the angular momentum leads to ℓ and m. For a perfect sphere there is no particular quantization axis; this leads to m independence, corresponding to a degeneracy in m for the resonances. We can note that the radial equation:

$$\frac{\mathrm{d}^2 f_\ell(r)}{\mathrm{d}\, r^2} + \left[N^2(r)k^2 - \frac{\ell(\ell+1)}{r^2}\right] f_\ell(r) = 0 \tag{17}$$

is very similar to the Schrödinger equation of a particle with a mass M in a pocket-like pseudopotential V_{eff} (depending from energy)

$$\left[-\frac{\hbar^2}{2M}\Delta_r + V_{\mathrm{eff}}(r)\right]\psi(r) = E\psi(r), \tag{18}$$

where $E = \frac{\hbar^2k^2}{2M}$ and

$$V_{\mathrm{eff}}(r) = \frac{\hbar^2}{2M}\left\{\left[1-N^2(r)\right]k^2 + \frac{\ell(\ell+1)}{r^2}\right\}. \tag{19}$$

This pseudopotential takes into account the refractive index discontinuity $N-1$ at the surface of the sphere and its curvature. This effective potential approach thoroughly analyzed by Nussenzveig [45] provides good physical insight into many properties of the WGMs that appear as quasibound states of light, analogous to the circular Rydberg states of alkali atoms. The number of peaks in the radial distribution of the field inside the sphere (Fig. 2) leads naturally to a radial number n. It corresponds directly to the radial index we can find with the Eikonal approach [46, 47]. The lowest-lying state is confined near the bottom of the potential well, i.e. as close as possible to the surface of the sphere (Fig. 3), and is expected to occur for $\ell \approx Nka \approx Nx$, the maximum value of the angular momentum. Light trapped into this mode can escape out of the sphere only by tunneling across the potential barrier that extends as far as Na for this state. The very long evanescent tail of this quasibound

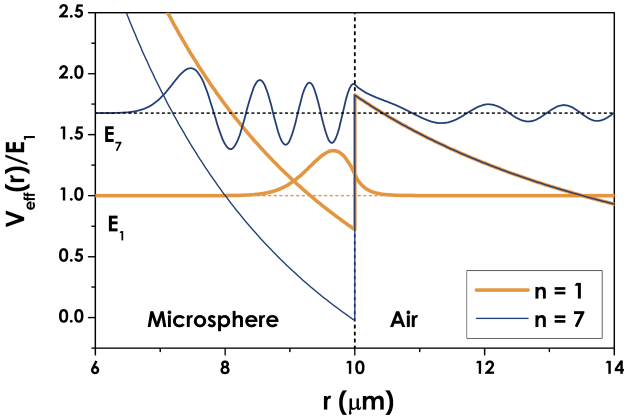

Figure 2 (online color at: www.lpr-journal.org) Effective potential and radial functions associated with, for an equivalent particle and turning point for fundamental energy E_1 (n = 1) and E_7 (n= 7) in the case of a TE mode (ℓ = 100) in a silica sphere (a = 10 μm, N = 1.45).

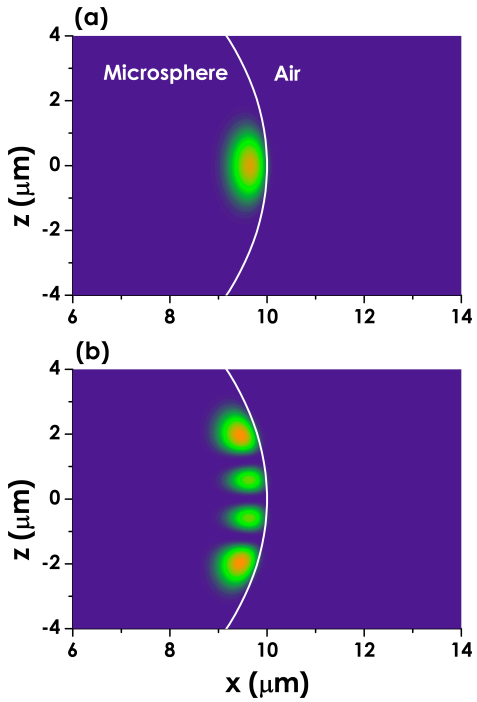

Figure 3 (online color at: www.lpr-journal.org) Poynting's vectors for a TE mode (n = 1, ℓ = 100) in a silica microsphere (a = 10 μm, N = 1.45) – (a) mode $|\ell - m|$ = 0 – (b) mode $|\ell - m| = 3$.

state implies a very weak coupling to the outside medium (usually air; $N = 1$) and extremely high Q factors. The quasibound state energy domain is limited; thus, only few n values correspond to WGM.

From Eq. (16) we deduce the main properties of a WGM spectrum. By analogy with a Fabry-Perot interferometer, we can define a pseudofree spectral range (pseudo-FSR) of the cavity $\Delta\nu_{n,\ell}^{\Delta\ell} = c(x_{n,\ell+1} - x_{n,\ell})/2\pi a$, which corresponds to the spacing between two modes with the same polarization and with the same n but which only differ by one unit of their quantum number ℓ. To a first approximation:

$$\Delta\nu_{n,\ell}^{\Delta\ell} \approx \frac{c}{2\pi N a}\,. \tag{20}$$

We can also derive the spacing between two adjacent modes labeled as TE and TM and with fixed values of n and ℓ:

$$\Delta\nu_{n,\ell}^{\mathrm{TE,TM}} \approx \frac{c}{2\pi N a}\frac{\sqrt{N^2-1}}{N}\,. \tag{21}$$

From an experimental point of view, the fabricated resonators are never perfect spheres but they can be considered to a first approximation as spheroids (oblate or prolate). We define the ellipticity of this spheroid by $e = (r_p - r_e)/a$ where r_p and r_e are, respectively, the polar (r_p) and equatorial (r_e) radii. For given n and ℓ values, considering a low ellipticity and $|\mathrm{m}| \approx \ell$, the relative frequency shift with respect to the spherical case is:

$$\frac{\Delta\nu_{n,\ell,m}}{\nu_{n,\ell}^{0}} = -\frac{e}{6}\left(1 - 3\left(\frac{|m|}{\ell + 1/2}\right)^2\right)\,. \tag{22}$$

In a recent paper Gorodetsky and Fomin [47] used the Eikonal method to analyze, as a practical example, a spheroidal dielectric cavity and they showed how the geometrical interpretation allows one the expansion of the method on arbitrarily shaped axisymmetric bodies.

2.3. *Quality factor*

Whispering-gallery modes are not only supported by spheres but also by cylindrical, spheroidal and toroidal-shaped open dielectric resonators. All these WGM resonators can have an extremely high quality factor, that makes them promising devices for applications in optoelectronics and experimental physics. In order to characterize the property of a resonator to keep inside its energy for a time τ, it is usual to introduce the resonance quality factor Q defined as:

$$Q = \frac{\omega}{\Delta\omega} = \omega\tau, \tag{23}$$

where $\Delta\omega$ is the linewidth (FWHM) associated with the considered resonance. Table 1 gives some examples of measured Q factors for different kinds of WGM resonators and different materials (fused glasses and crystals).

For an isolated (not coupled) WGM resonator, we can identify four independent contributions to its intrinsic Q factor Q_0:

$$Q_0^{-1} = Q_{\mathrm{rad}}^{-1} + Q_{\mathrm{mat}}^{-1} + Q_{\mathrm{s.s}}^{-1} + Q_{\mathrm{cont}}^{-1}\,. \tag{24}$$

The first term Q_{rad} denotes radiative (curvature) losses, and corresponds to the escape of energy through the potential

Table 1 Order of magnitude of measured Q factors associated with passive whispering-gallery resonators differing in shape and materials.

Geometry of the resonator	Material	Q factor	Ref.
Sphere	silica	10^8–10^9	[48]
Spherical droplet	Rhodamine 6G in water	10^8	[40]
Torus	silica	10^8	[28]
Truncated spheroid	CaF_2	10^{11}	[49]
Truncated spheroid	MgF_2	10^8	[50]

barrier and by using a semiclassical (WKB) approximation for the Riccati-Bessel radial solutions, one can find [51]:

$$Q_{\mathrm{rad}} \cong x\, \mathrm{e}^{2(\ell+1/2)g\left(\frac{x}{\ell+1/2}\right)}, \tag{25}$$

with $g(y) = -\sqrt{1-y^2} + \arg\cosh(1/y)$ and x the size parameter. Taking into account low radial orders (in this case $x/\ell \approx 1/N$)g can be replaced by its tangent, which leads to:

$$Q_{\mathrm{rad}} \cong \ell/N \exp\left[+2\ell g\left(\frac{1}{N}\right)\right] \times \exp\left[-2\sqrt{N^2-1}\frac{Nx-\ell}{N}\right]. \tag{26}$$

Using Eq. (16) we can develop an expression depending from the radial order n and polarization TE or TM. This approximation shows that Q_{rad} decreases as n increases and that for a given mode the Q factor associated with the TM polarization is slightly lower than the value associated with the TE polarization. Q_{rad}^{-1} vanishes exponentially with increasing size, so with $D/\lambda \geqslant 15$, $Q_{\mathrm{rad}} > 10^{11}$ (D is the microsphere diameter; λ is the wavelength) and the diffraction losses can be considered as negligible with respect to absorption losses if we consider well confined modes ($n = 1, 2, 3\ldots$).

Q_{mat} is associated with absorption and bulk Rayleigh scattering in the material constituting the microresonator. Considering an attenuation α in dB/km, Q_{mat} can be approximated by:

$$Q_{\mathrm{mat}} \cong \frac{4.3\times 10^3}{\alpha}\frac{2\pi N}{\lambda}. \tag{27}$$

For an undoped silica glass ($\alpha = 0.17$ dB/km at $\lambda = 1.55\,\mu$m) it turns out that $Q_{\mathrm{mat}} \cong 10^{11}$.

$Q_{\mathrm{s.s}}^{-1}$ denotes scattering losses due to residual surface inhomogeneities. Calculations based on the model of Rayleigh scattering by molecular-sized surface clusters [52] under grazing incidence and total internal reflection yield the following estimate for $Q_{\mathrm{s.s}}$ [48]:

$$Q_{\mathrm{s.s}} = \frac{\lambda^2 D}{2\pi^2\sigma^2 B}, \tag{28}$$

where σ and B are the rms size and the correlation length of inhomogeneities. With the numerical values reported for glass surfaces [53] we conclude that $Q_{\mathrm{s.s}} \gg 10^{10}$ can be expected only in large spheres ($D \gg 100\,\mu$m).

Q_{cont}^{-1} denotes the losses introduced by surface contaminants during the fabrication process. Gorodetsky et al. [48] demonstrated how, in fused-silica microresonators, the ultimate Q factor is limited by adsorption of atmospheric water on the surface.

3. Fabrication of spherical microresonators

One of the great advantages of microspheres is that they may be very easily produced in a laboratory setting from a large variety of materials, organic and inorganic. Here attention will be focused onto the fabrication of glass microspheres. Fig. 4 shows an optical micrograph of a silica microsphere, attached to the fiber stem from which it was formed. From the point of view of the resonator, the presence of the stem can usually be ignored as the excited optical modes typically lie in the equatorial plane and thus have negligible overlap with this perturbation region.

Two main techniques for the fabrication of glass microspherical resonators can be taken into consideration, one based on melting processes, the other one on sol-gel chemistry.

Figure 4 (online color at: www.lpr-journal.org) Upconversion green image mapping the optical pump WGMs in an erbium-doped phosphate microsphere with a diameter of approximately 150 micrometers.

3.1. Melting processes

General-purpose processes, which can be used to fabricate microspheres from a large range of glass compositions, imply either directly producing a glass by melting or using the powder obtained by crushing an available glass. In the first case, several paths can be followed: a very simple one, which has also been used to fabricate Er^{3+}-doped tellurite glass microlasers, consists of melting the oxide components in a furnace and dropping the viscous glass on a spinning plate [54]. Another process, adopted for a multicomponent fluoride glass based on ZrF_4, started from melting the raw materials in a vitreous carbon crucible at 1000 °C, in an induction furnace; then, the molten batch was poured in a fine stream into liquid nitrogen, and the spherical particles that passed through a 50-mesh sieve were collected from the quenched glasses [55]. A problem occurring in such a case was the easy contamination of the sphere surface, in particular by oxidized products, such as Zr–OH and Zr–O; a chemical polishing was therefore required, and it was performed by using an ultrasonically agitated bath of $ZrOCl_2$–$8H_2O$ dissolved in water. All the operations, except the chemical polishing, were carried out in a dry nitrogen gas atmosphere.

A much more complex approach, that we report here for the sake of completeness, is represented by the use of the magnetic levitation method: containerless melting of glass and fabrication of microspheres from a cubic glass sample (e.g. with a size of 4 or 6 mm) in a furnace constituted by a CO_2 laser and a solenoid-type magnet was demonstrated [56, 57]. The glass cube, placed in a platinum cage at the edge of the inner magnet, is made to levitate and there it is melted by the effect of the focused laser beam: a complete glass sphere was thus obtained after cooling. Subsequent polishing to optical grade, however, seems to be necessary [57].

In the second type of general fabrication process, a glass is crushed and then its powder is dropped through a microwave plasma torch [58]: the remelted glass grains acquire spherical shape by surface tension before being hardened by the air flow and falling into a proper container. By adjusting the microwave power and the gas flow, it is possible to reach the desired temperature (around 2000 °C for silica-based glasses, 800–900 °C for fluoride glasses), and to produce spheres with a low eccentricity.

With the exception of the magnetic-levitation method, which on the other hand requires the previous preparation of a cube with the desired size, a disadvantage of these techniques is that one obtains a number of free spheres with a large size distribution that are difficult to manipulate. It is therefore necessary to place the produced spheres under an optical microscope and to sort them by size, while also checking their surface quality. The selected spheres may be picked up with a commercial glass capillary connected to a vacuum pump, and then, one at a time, stuck on a tapered fiber, as shown in Fig. 5.

A very simple and effective method is the one based on the melting of the end of a glass fiber. It presents the disadvantage of requiring a glass in form of rod or fiber and of permitting the fabrication of only one microsphere at a time, but it is very cheap and allows one a very good control of the microsphere diameter. Upon heating the distal tip of a fiber, e.g. a standard telecommunications silica fiber, the glass reflows to form a spherical volume under the influence of surface tension. Due to the high viscosity of silica, the reflowed structure becomes highly spherical (eccentricities of the order of 1–2%), and extremely uniform. The spherical surface has very low intrinsic roughness (we measured rms roughness of the order of 1 nm), and thus has a very small surface scattering loss.

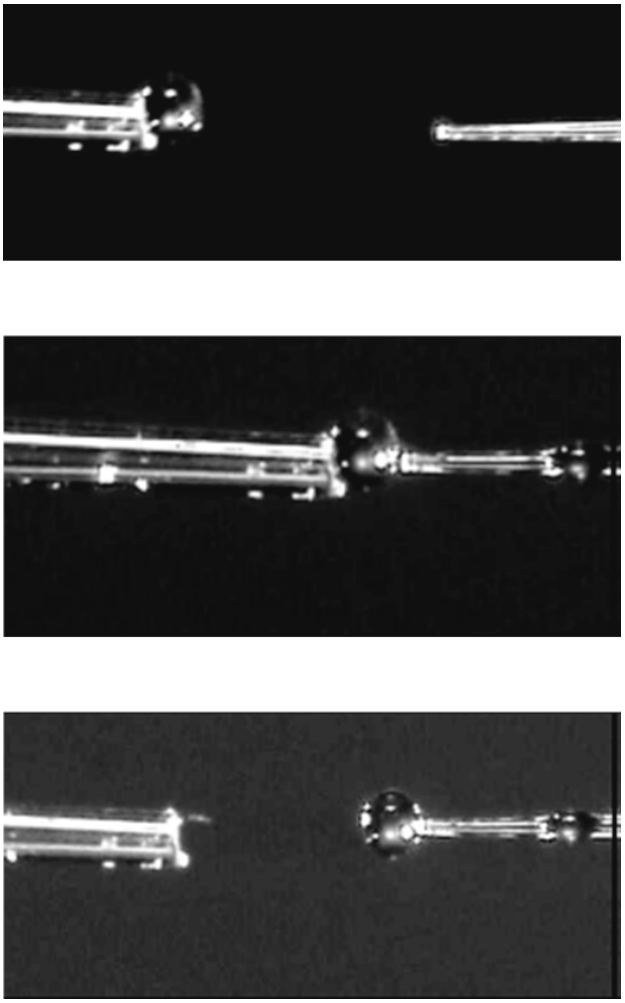

Figure 5 Microphotographs of three successive steps of mounting a melted glass microsphere onto a tapered fiber having a very thin layer of glue onto the tip (on the left: the draft capillary tube; on the right: the fiber tip).

The reflow process may be induced using different heating sources: an oxygen/butane (or similar) torch, a high-power (e.g. a CO_2) laser [59, 60], or an electric arc as in a commercial fiber splicer [61]. Fiber splicing is a mechanic-thermal process in which the cleaved fiber ends are heated to a temperature at which they soften. By accurately control-

ling the operating parameters of the splicer, reproducible spherical shapes are easily obtained. These techniques allow one to produce microspheres with diameters usually in the range d to $1.5d$, where d is the outer diameter of the uncoated fiber; smaller spheres, say from 20 to 100 µm in the case of conventional telecom fibers, may be obtained by first tapering the fiber in order to reduce the diameter of the tip.

3.2. Sol-gel processes

Sol-gel chemistry has attracted increasing interest in recent years as a very flexible and cheap method for producing optical materials. The possibility of starting from molecular precursors and elementary building blocks permits the tailoring of structures at the molecular level and creating new materials with enhanced performances.

Two major approaches can be followed when using sol-gel processes to produce spherical microresonators. In fact, besides synthesizing a "bulk" glass with a spherical shape, one can deposit a uniform sol-gel film onto a microsphere previously produced by heating process; Yang et al. demonstrated that it is possible to excite WGMs in a thin film deposited on a passive microsphere and to obtain a laser effect [59].

Many protocols can be used to realize sol-gel silica spheres: monodisperse silica nanoparticles, in particular, can easily synthesized via the base-catalyzed hydrolysis of TEOS [62]; the silica spheres may have a diameter in the range from 150 nm to 2 µm, with typical size dispersion around 3%. This method cannot be used if one wants to incorporate rare earths into the glass, because lanthanide salts form insoluble lanthanide hydroxides in basic environments. The problem, however, may be overcome by using acid catalysts [63, 64]: in this case one obtains silica microspheres with different diameters, ranging from a hundred nanometers to approximately 150 micrometers, always with a very high surface quality, as shown by the TEM images in Fig. 6.

The second approach to produce sol-gel-based microspherical resonators takes advantage of the capability of sol-gel solutions to produce very high quality thin films. A pure-silica microsphere can be thus coated, e.g. by the dip-coating method [61]. The microsphere is fixed to the dipping bar of the coating system (Fig. 7). After each dip, the microsphere is put into a furnace (or equivalent annealing apparatus) in order to remove the solvent; the operation is repeated a number of times in order to obtain the desired thickness of the film. As a result of the procedure, a crack-free functional film, which may act as the effective microcavity, is obtained.

Another method used to coat spherical microspheres is based on a dispersion process [65]. In this case the spheres are dispersed in the sol-gel solution and soaked in it. The solution is then filtered and the coated spheres are taken out of the membrane filter and dried; the process is sketched in Fig. 8.

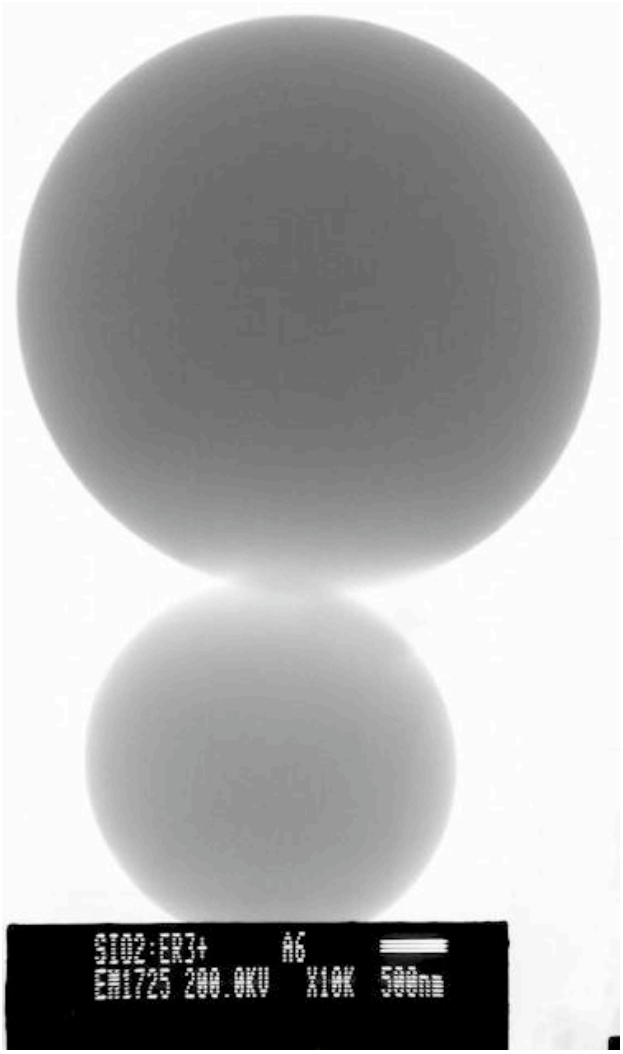

Figure 6 TEM image of two sol-gel silica microspheres (the reference bar indicates 500 nm).

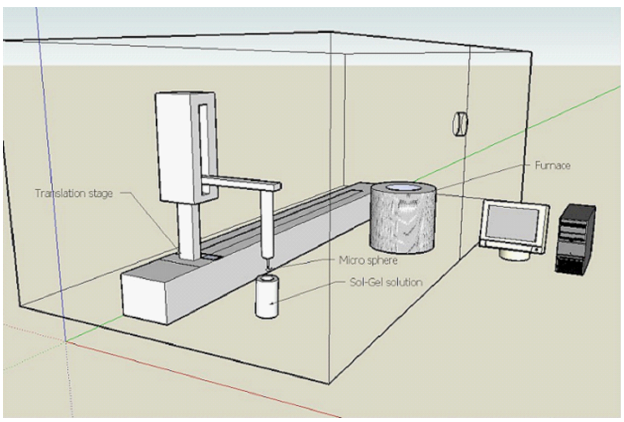

Figure 7 (online color at: www.lpr-journal.org) Sketch of the experimental apparatus for sol-gel dip coating of pure-silica microspheres.

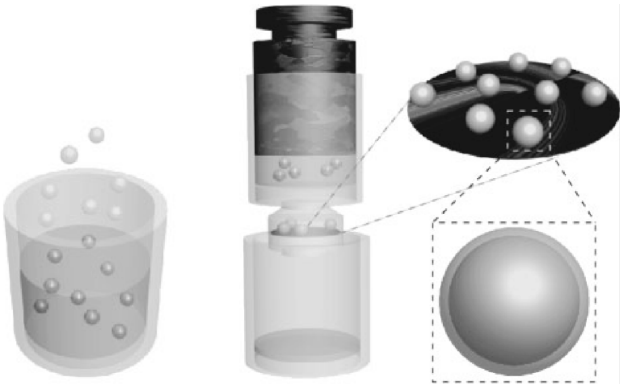

Figure 8 Representation of the dispersion process steps to coat microspherical beads. From the left: beads are dispersed in the sol-gel solution; the solution is filtered; the membrane filter is removed and coated microspheres may be used after drying.

Sol-gel-produced spheres present the advantage of very high purity materials; moreover, composition of bulk and film microresonators may be tailored according to the application.

4. Light coupling into microspheres

In order to fully exploit the potential of microspheres for fundamental investigations as well as for practical applications the most critical point is an efficient, controllable, and robust coupling to the cavity WGMs. The only approach that fulfils these operational principles is based on phase-matched evanescent field coupling. This technique requires an overlap of the evanescent field of the WGM with the evanescent field of the coupler; an effective excitation of the mode(s) is possible when the phase-matching conditions are satisfied as well.

4.1. Coupling systems

The most commonly used coupling systems to inject light into a microsphere are depicted in Fig. 9: they are based on evanescent-wave coupling either from an adjacent guiding structure such as an optical fiber (a) and a channel waveguide (b), or from a prism (c) and an angle-polished fiber (d) under TIR.

The tapered fiber [66–68] is an excellent and easy-to-align coupling tool that allows fine tuning of the fiber mode propagation constant by controlling the taper thickness. Fiber tapers are commonly fabricated by heating and at the same time slowly pulling a section of the fiber to form a narrow waist. Advanced fiber splicing equipment or specific cylindrical microfurnaces are used for this purpose. The appropriate taper waist can be as small as a micrometer in diameter, with the fundamental mode extending significantly into the free space surrounding the taper. The typical total length of the adiabatic tapered section is more than 1 cm. A critical point for fiber couplers is the fact that the tapered region is very thin and therefore very fragile and easy to deteriorate.

The integrated waveguide coupler [69] consists of a properly designed phase-matched surface-channel waveguide whose evanescent field overlaps with the microsphere WGMs. Achieving an efficient coupling is rather critical and requires a careful alignment, but the system is more compact and robust than the fiber taper.

Prism-to-sphere coupling [70] is among the earliest concepts. A laser beam is directed into a prism and undergoes TIR at the prism surface. The resulting evanescent optical field at the prism surface can then be coupled into the spherical resonator. Phase matching is obtained by selecting the proper incidence angle. The system is rather robust, but achieving optimal alignment is quite challenging.

The fiber-prism coupler [71] combines the advantages of waveguide light insertion with the robustness of prism coupling. A fiber end is polished along a specific angle that allows phase matching. This angled plane then acts as a TIR surface for the light guided into the fiber, that can thus be coupled to the microsphere. The fiber-prism method eliminates part of the alignment steps that are necessary for bulk prism couplers. It is worth noting that in the tapered fiber or waveguide coupling systems the transmitted light, after the interaction with the microsphere, is still conveniently

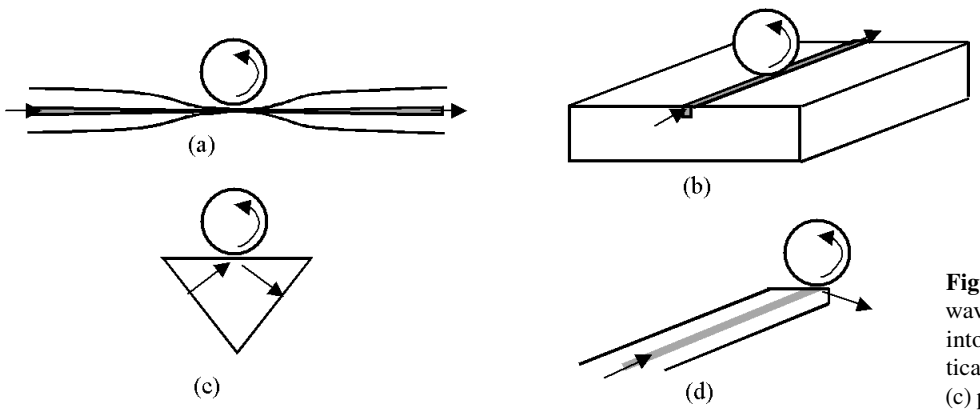

Figure 9 Schemes of evanescent-wave couplers used to inject light into a microsphere. (a) Tapered optical fiber, (b) integrated waveguide, (c) prism and (d) angle polished fiber.

guided into the same fiber or waveguide, while in the other approaches it propagates in free space.

Once the light has been coupled inside the microsphere, a portion of it can be extracted by using a second evanescent coupler (output coupler) that indeed collects a portion of the intracavity signal. Another approach to directly monitor the light inside the resonator is to collect part of the light scattered at the resonator surface with a microscope objective or a multimode fiber.

4.2. Coupling analysis

In order to analyze the coupling of light to a microsphere we refer to the simple scheme sketched in Figs. 10a (top view) and b (cross section), where we assume that one mode propagating into the waveguide is coupled to a microsphere WGM whose propagation constant is β ('ideality coupler' [72]). E_i and E_o are the amplitudes of the waveguide electric field before and after the interaction with the spherical microcavity, respectively. In analogy with a mirror in a Fabry-Perot cavity, let t be the coupling coefficient from the fiber to the microsphere and r be the portion of the field in the waveguide transmitted after the coupling region, with $r^2 - t^2 = 1$ (t is purely imaginary). Considering the phase and amplitude contributions for each round trip [73], we can write the ratio between the intensity of the light lost and scattered by the microsphere I_s and that at the input of the coupling section I_i:

$$\frac{I_\mathrm{s}}{I_\mathrm{i}} = 1 - \frac{I_\mathrm{o}}{I_\mathrm{i}} = 1 - \left\| \frac{E_\mathrm{o}}{E_\mathrm{i}} \right\|^2 = \frac{T_\mathrm{m}}{1 + F^2 \sin^2(\beta L/2)} \quad (29)$$

where T_m is expressed by:

$$T_\mathrm{m} = 1 - \left(\frac{r - \mathrm{e}^{-\alpha L}}{1 - r\,\mathrm{e}^{-\alpha L}} \right)^2 , \quad (30)$$

and F is the finesse of the spherical microcavity, defined as:

$$F = \pi \frac{\sqrt{r\,\mathrm{e}^{-\alpha L}}}{1 - r\,\mathrm{e}^{-\alpha L}} . \quad (31)$$

α is the attenuation coefficient of the WGM and accounts for all type of sphere intrinsic losses, $Q_0 = \beta/(2\alpha)$ being the intrinsic quality factor (also defined by Eq. (23)), and $L = 2\pi a$ the circumference of the sphere. Eq. (29) is analogous to that of a linear Fabry-Perot cavity with unequal mirrors, one of them reflecting 100% of the light. T_m is the magnitude of the resonance peaks – when $\beta L = 2\pi\ell$ with ℓ integer – and its maximum value is $T_m = 1$ when $r = \mathrm{e}^{-\alpha L}$. At resonance, this latter condition corresponds to the so-called critical coupling with the transmission dip going down to zero.

Under the condition of low cavity round trip losses ($\alpha L \ll 1$) and reduced coupling $|t|^2 \ll 1$, the composite waveguide-sphere quality factor Q can be derived from Eq. (29) in the simplified form [74]:

$$\frac{1}{Q} = \frac{1}{Q_0} + \frac{1}{Q_\mathrm{e}} , \quad (32)$$

where the loading (external) factor $Q_\mathrm{e} = 2\pi a\beta/|t|^2$ accounts for the coupling losses and is proportional to the inverse of the transmittance of the coupler.

Coupling is also characterized by the fractional depth K of the resonance dip in intensity transmittance through the coupler. K is observed upon varying the frequency of the exciting wave around the resonance and under resonance conditions can be expressed as a function of the intrinsic quality factor of the WGM Q_0 [74]:

$$K = 4\Gamma^2 \frac{Q_0 Q_\mathrm{e}}{(Q_0 + Q_\mathrm{e})^2} , \quad (33)$$

where the coefficient Γ describes mode matching (a single-mode coupler is always mode matched). Unlike the case of Fabry-Perot cavities with their fixed coupling to external beams, the sphere-coupler system provides a unique opportunity to easily control the bandwidth of the cavity (as an input mirror with variable transmittance). In fact, Q_e can be adjusted by increasing the gap between the coupler and the sphere from the overcoupled regime ($Q_\mathrm{e} < Q_0$) to the undercoupled one ($Q_\mathrm{e} > Q_0$), which permits a clear observation of saturation of the measured Q up to the intrinsic (unloaded) value Q_0. Maximum contrast is achieved under critical coupling when coupling losses equal intrinsic cavity losses, i.e. $Q_\mathrm{e} = Q_0$ or $Q = 1/2Q_0$, and the entire coupled power is lost inside the resonator [76, 77].

Fig. 11a shows the measured Q values for increasing values of the gap between a fiber taper with a 4-μm waist and a 250-μm silica microsphere; Q tends to the saturation

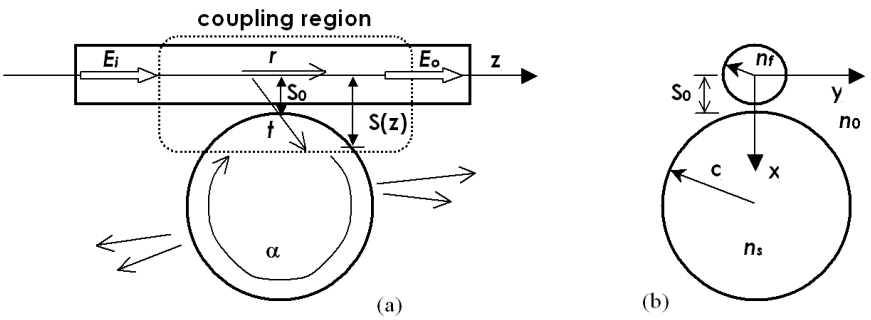

Figure 10 Scheme of a waveguide or fiber to microsphere coupling system: (a) top view and (b) cross-sectional view.

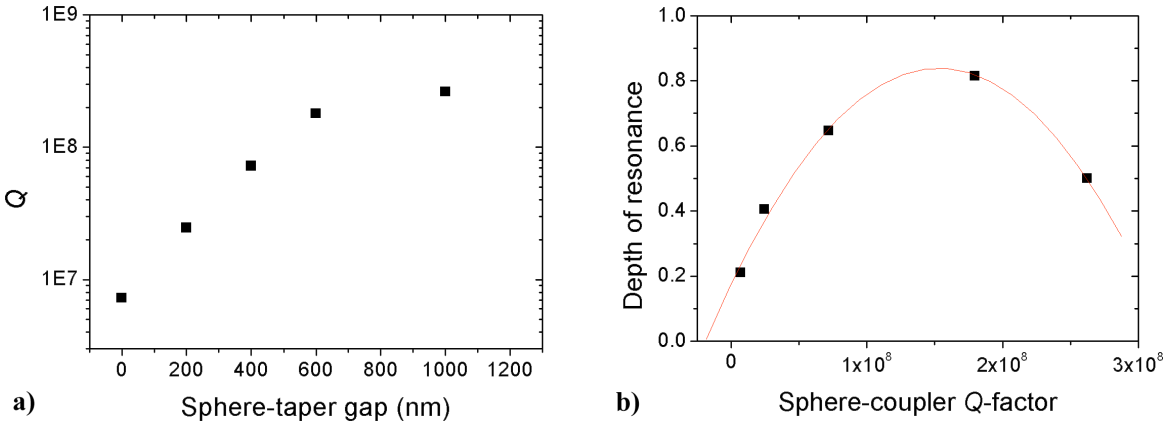

Figure 11 (a) Measured Q values vs. fiber-microsphere gap. Q factor saturates to its intrinsic value $Q_0 \sim 3 \times 10^8$. (b) Depth of resonance K vs. sphere-coupler system Q factor.

value close to its intrinsic value Q_0 of about 3×10^8 when the gap is around 1 μm [75]. Fig. 11b plots the contrast K (or depth of the resonance of the WGMs) versus the Q factor. In agreement with the theory described above, the maximum resonance contrast is achieved when coupling losses equal intrinsic cavity losses, i.e. $Q = 1/2Q_0 = 1.5 \times 10^8$. In this case the maximum value of K is less than 1 (~ 0.8) because the 4-μm taper has multiple modes that can be excited (they will not be all matched to the microsphere WGM), and also the polarization state is arbitrary.

The cross-sectional view of a tapered fiber (or a waveguide) evanescently coupled to a sphere is depicted in Fig. 10b. $S(z)$ is the distance between the sphere surface and the fiber axis, and S_0 is its minimum. The interaction strength κ between the fiber mode F_0 and the sphere WGM $\Psi_{n,l,m}$ is given by the following overlap integral:

$$\kappa\left(S\left(z\right)\right) = \frac{k^2}{2\beta_{\mathrm{f}}} \int_x \int_y \left(n_{\mathrm{s}}^2 - n_0^2\right) F_0 \psi_{n,l,m} \,\mathrm{d}\, x \,\mathrm{d}\, y \,, \quad (34)$$

where β_f is the propagation constant of the fiber mode, and integration is carried out over the transverse extent of the sphere only. Due to the near-parabolic curvature of the sphere at the minimum separation the interaction decreases with a Gaussian dependency away from this point along the length of the fiber z. κ^2, i.e. the amount of power coupled out of the fiber into the sphere per revolution (equal to $|t|^2$), is found by integrating Eq. (34) along z [78]:

$$\kappa^2 = \kappa^2\left(S_0\right) \frac{2\pi a}{\gamma_{\mathrm{f}}} \exp\left(-\frac{a}{\gamma_{\mathrm{f}}}\left(\beta_{\mathrm{f}} - \beta_{\mathrm{s}}\right)^2\right) , \quad (35)$$

where γ_f is the fiber mode decay constant outside the taper boundaries and $(\beta_f - \beta_s)$ accounts for the modes phase mismatch.

4.3. Q-factor measurement

The Q values of the microspheres can be calculated from the measured resonance linewidth $\delta\nu$ of the excited WGM according to Eq. (23), which can also be written as $Q = \nu/\delta\nu$, where ν is the frequency. In this case the Q factor of the resonator is measured in the stationary regime. The experimental setup for this type of measurement is sketched in Fig. 12. The laser is finely swept at low frequency around a resonance so the linewidth of the laser sets the upper limit for the measurable Q factor**.** Coupling efficiency from the fiber taper to the microsphere can be gradually increased by reducing the gap between the sphere and the taper, thus affecting both resonance width and depth, as discussed previously. The transmission at the output of the taper is monitored using a photodiode detector connected to an oscilloscope that is controlled by a PC where data can be recorded.

A typical resonance around 1550 nm for a silica sphere is shown in Fig. 13 together with a Lorentzian fit. In this case Q is equal to 2.6×10^8 and K is 0.5 (this value corresponds to the last point in the plot of Fig. 11b) [75]. We used a tunable external-cavity laser with linewidth of a few hundred kHz as light source. The light transmitted through the coupler-microsphere system is measured at the output of the taper using an amplified InGaAs photodiode detector connected to a 1-GHz oscilloscope. The silica sphere has a diameter of 250 μm, while the fiber taper waist is 4 μm.

The intrinsic limit of Q factor measurement in the stationary regime from the resonance linewidth (i.e. due to laser linewidth and thermal effects) can be overcome using the same setup but sweeping the laser frequency with the proper speed across the resonance. It has been shown that a fast sweeping of the cavity resonance or of the excitation wavelength induces a ringing phenomenon (as in cavity ring down spectroscopy) [79–82]. This can be exploited to easily measure ultrahigh loaded Q factors avoiding stationary technique drawbacks for high-finesse resonators [83–86] or whispering-gallery mode (WGM) resonators [49, 87]. A

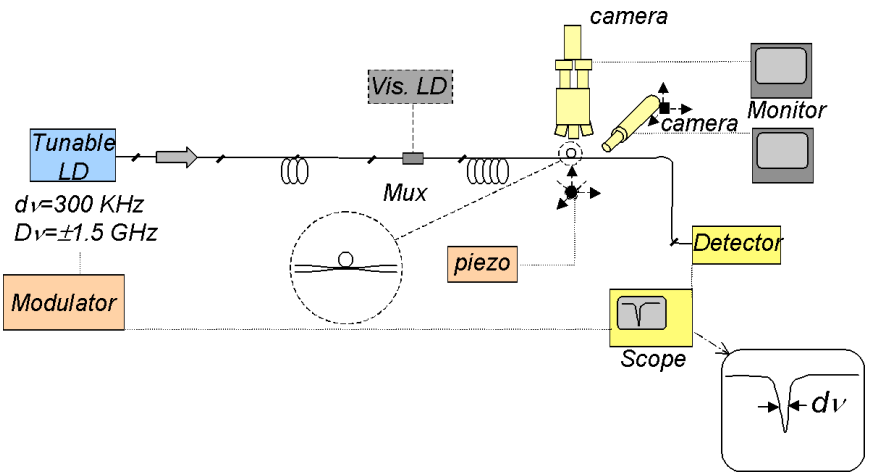

Figure 12 (online color at: www.lpr-journal.org) Experimental setup for Q factor measurement.

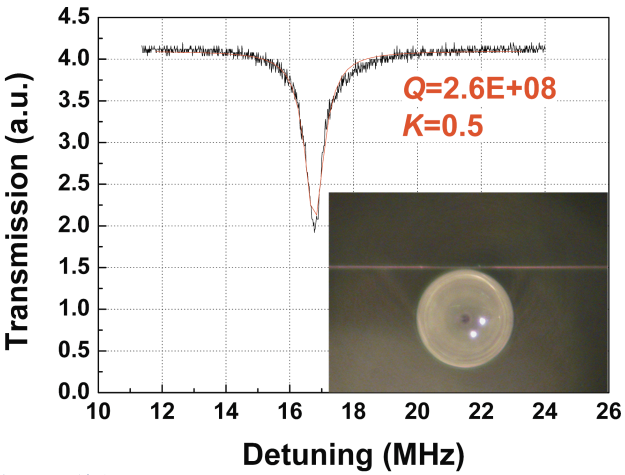

Figure 13 (online color at: www.lpr-journal.org) WGM resonance of a silica sphere with a diameter of 250 µm coupled to a 4 µm waist-tapered fiber. Red line indicates the Lorentzian fit.

part of the light is accumulated first and then re-emitted, thus interfering with the laser light and generating a beatnote signal like the one shown in Fig. 14a. The envelope of the decaying oscillations (Fig. 14b) follows the decay of the amplitude of the re-emitted light (equal to 2τ) [49, 50, 87].

Another method to assess the quality factor is based on the transient response or cavity ringdown measurement technique. By observing the output power decay after the input of a short pulse, Q is determined from the decay time τ (according to the equation $Q = 2\pi\nu\tau$) [88].

5. Spectroscopic and structural assessment

Compositional properties and fabrication processes play a capital role in determining the optical and spectroscopic properties of microspheres; photoluminescence and Raman spectroscopies represent two powerful tools for qualitative and quantitative study of microresonators, especially when activated by luminescent ions [89–91].

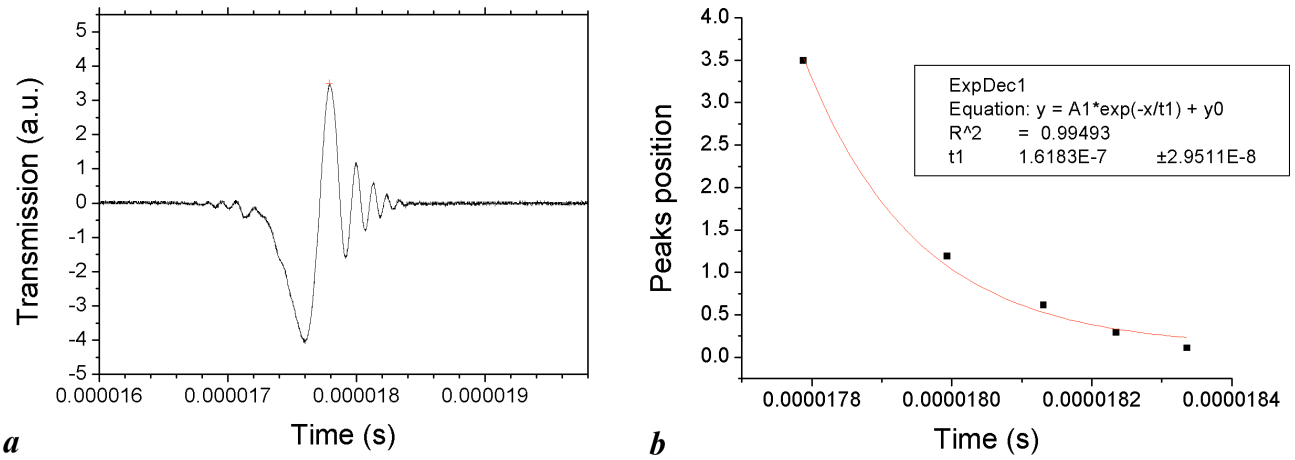

Figure 14 (online color at: www.lpr-journal.org) (a) Beatnote signal obtained sweeping the laser frequency rapidly across the resonance; (b) the corresponding envelope of the decaying oscillations.

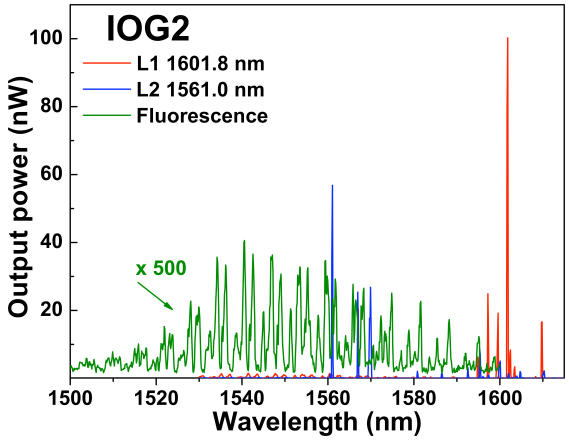

Figure 15 (online color at: www.lpr-journal.org) Emission spectra from a 70- µm microsphere made of Schott IOG2 glass. The luminescence spectrum was measured with a wavelength bandwidth of 0.1 nm.

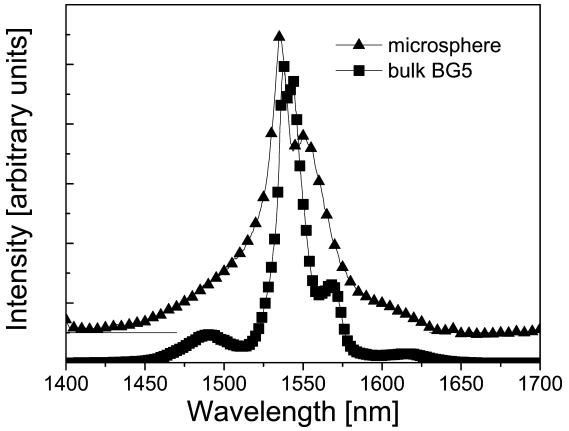

Figure 16 RT photoluminescence spectra of the $^4I_{13/2} \rightarrow {}^4I_{15/2}$ transition of Er^{3+} ions for the BG5 glass (squares) and the corresponding microsphere (triangles).

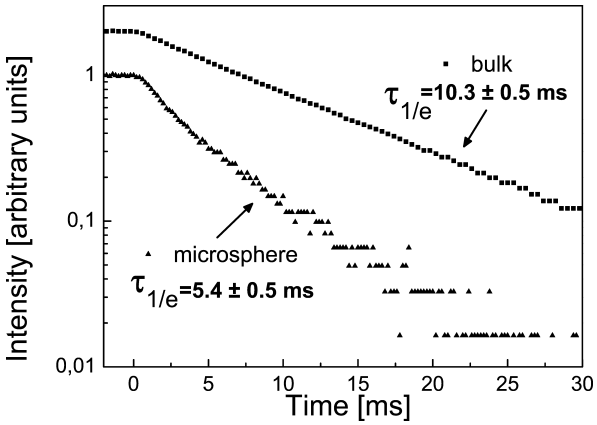

Figure 17 RT luminescence decay curves of the $^4I_{13/2}$ state of Er^{3+} ions for the BG5 glass (squares) and the corresponding microsphere (triangles).

As WGM microspherical resonators play an important role in the pursuit of compact and efficient laser sources, because of their intrinsic potential for low lasing threshold and narrow spectral characteristics, photoluminescence spectroscopy is a must. After the pioneering studies in the 1960s, when laser action was demonstrated in Sm:CaF_2 crystalline resonators [15], rare-earth-doped glass microresonator lasers have been intensively studied during the last decade [54, 58, 92–99]. Let us focus here on the $^4I_{13/2} \rightarrow {}^4I_{15/2}$ transition at 1.55 µm of Er^{3+} ions. In this case it is possible to follow the luminescence spectra in the infrared region modulated by the whispering-gallery modes. Fig. 15 shows the emission spectra from a 70- µm diameter microsphere made of Schott IOG2, a commercial erbium-ytterbium codoped phosphate glass; the green solid line shows the fluorescence, with a series of peaks that can be assigned to several families of WGMs. When increasing the pump intensity above a minimum threshold of 2.5 mW we obtained laser oscillation, corresponding to the red (L1) and blue (L2) lines.

Far-field excitation and standard photoluminescence analysis also provide significant information. As an example, we report here some results obtained in Er^{3+}-activated microspheres fabricated by a modified silica glass provided by the Baccarat factory [58]. Samples doped with 0.2, 0.5, and 1.5 at% of Er^{3+} were labeled as BG2, BG5 and BG15, respectively. Each bulk glass sample was crumbled, and microspheres were then fabricated using the plasma torch method previously described. Microspheres with diameter in the range 50 to 100 µm were selected and then glued to the tip of as many optical fibers; the chosen fiber was then mounted on a translation stage with piezoelectric actuators and a positioning resolution of 40 nm. Photoluminescence spectroscopy, in the region of the $^4I_{13/2} \rightarrow {}^4I_{15/2}$ transition of Er^{3+}, was performed using the 980.8-nm line of a Ti:sapphire laser as excitation source with a power of 450 mW. The luminescence was dispersed by a 320-mm single-grating monochromator with a resolution of 2 nm. The light was detected using a Si/InGaAs two-color photodiode and standard lock-in technique. Decay curves were obtained by recording the signal on a digital oscilloscope. For both the precursor glass and the microsphere the standard bulk measurement configuration was used. The laser beam directly excited the sample and the luminescence was recorded at 90° from the laser direction. As an example, Figs. 16 and 17 show the room-temperature (RT) photoluminescence spectrum and the corresponding luminescence decay curve, respectively, both for the glass precursor and the microsphere, in the case of the BG5 sample.

In the BG5 sample, more than in the other two, the differences of spectroscopic properties between the precursor glasses and the corresponding microspheres are evident. A significant broadening of the photoluminescence spectrum occurs in the microsphere: it is very likely that it is due to site-to-site inhomogeneities, induced by the fabrication pro-

cess. Because of the restricted number of samples, however, it is impossible to determine the specific reason of the induced inhomogeneity. It is possible that a further annealing, performed on the spheres at temperatures close to the glass transition temperature T_g, could reduce the local strains as well as the site inhomogeneities, as happens with massive glass. The difference in the local environment of the Er^{3+} ion in the microsphere results in an important modification of the transition probability among the Stark levels. The lifetime measurements give further information about the site-to-site inhomogeneities: indeed, the $^4I_{13/2}$ decay curves of Er^{3+} ion in the microspheres show a faster relaxation as compared to the bulk, indicating that the energy-transfer mechanism among active ions is effective in the microspheres at all Er^{3+} concentrations. One can conclude that the microsphere fabrication process can strongly affect the spectroscopic properties of the base glass, and that this has to be especially taken into account if one wants to use microspherical laser performances as a 'test bed' for the active glass itself.

Continuous-wave laser oscillation was also obtained in BG5 spheres, with a threshold of 2.5 mW. By varying the gap between the tapered fiber coupler and the microsphere and increasing the pump power, a shift of the laser spectrum towards WGMs of shorter wavelength was achieved. The laser emission ranged from 1569.3 nm to 1541.2 nm. This effect can be explained with a similar shift that occurs in the Er^{3+} gain spectrum when the inversion rate increases [100].

As far as the structural properties of glass microresonators are concerned, Raman spectroscopy may be very useful, especially for multicomponent glass systems [91]. This is particularly true in the case of silicate systems, where reports of a huge number of studies using Raman spectroscopy are available; another important application concerns cases where thermal annealing effects, like in the sol-gel fabrication process, have to be considered [64]. Let us refer to the latter case, and let us observe Fig. 18, where two micro-Raman spectra are reported. These spectra refer to a single silica sphere heat-treated at different temperatures, namely at 950 °C (a) and at 1100 °C (b). One can notice the presence of the Raman bands at about 440, 490, 600, 800, and 1060 cm^{-1}, all characteristic of the silica network [101]. Moreover, in the spectrum of Fig. 18a a band centered at about 970 cm^{-1} is present, attributed to the Si–OH vibration [101]. The comparison of Raman spectra indicates a modification of the structural properties of the spheres as a function of the annealing temperature. In fact, the spectrum (b) makes evident a decrease of the intensity of the band centered at 970 cm^{-1} as well as of the bands at 490 and at 600 cm^{-1}, which are attributed to the defects band D1 and D2, respectively [102, 103]. These observations confirm that when increasing the annealing temperature we promote a more complete condensation of the surface and interior silanol group, and an elimination of any adsorbed water, alcohol, or remaining acetate groups. Since a fully densified, dry material is of paramount importance for spherical microresonators, it is obvious that the higher annealing temperature is definitely preferable.

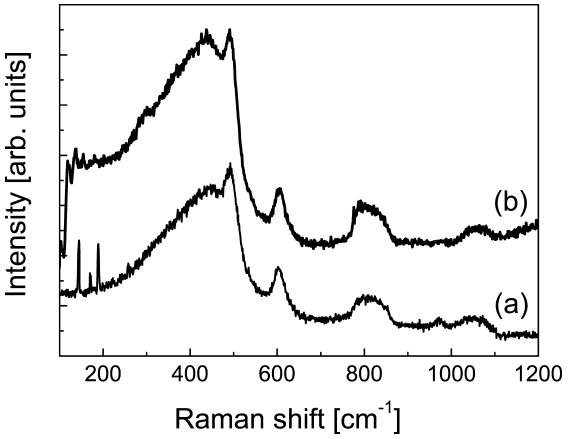

Figure 18 Micro-Raman spectra measured on a single silica microsphere, produced by the sol-gel process, heat treated at 950 °C (a) and 1100 °C (b).

6. Applications of spherical microresonators

The most common applications of generic optical resonators lay in the areas of laser cavities and resonant filters [18, 21, 22], but they are also used in sensors such as the laser gyroscope, and more generally in optical precision measurements. The miniature microsphere resonators, thanks to their extremely high quality factors, possess unique performance characteristics (extremely narrow resonant linewidth, long decay time and high energy density), and are therefore particularly well suited to a number of applications, that include, for instance, cavity-QED experimentation, detection and sensing, frequency stabilization, and optical filtering functions.

6.1. Biochemical sensors

According to the International Union of Pure and Applied Chemistry (IUPAC) an electrochemical biosensor is "a self-contained integrated device, which is capable of providing specific quantitative or semiquantitative analytical information using a biological recognition element (biochemical receptor) which is retained in direct spatial contact with a transduction element" [104]. The interaction produces an effect measured by the transducer, which converts the information into a measurable effect, in our case an optical signal. An important aim of much of the work done in (bio)sensing has been to develop disease detection systems with the longer-term goal of prevention.

The requirements for a biosensor are selectivity, sensitivity, stability and reversibility. These are mostly provided by the biochemical receptor, the sensitivity being also affected by the quality of the transducer. Equally important parameters are high signal-to-noise-ratio (SNR), short response time, low limit of detection (LOD), high sensitivity at low cost and in real samples. The main goals of a sensor

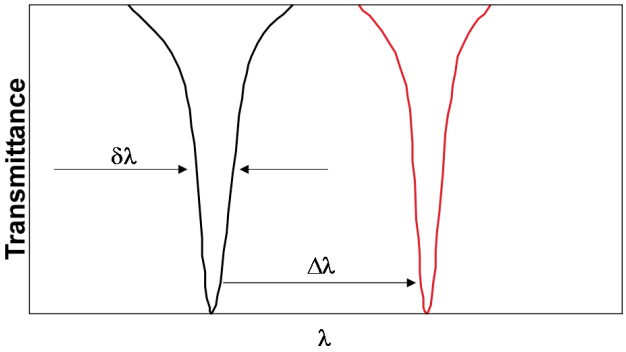

Figure 19 (online color at: www.lpr-journal.org) Resonance shift after analyte binding to the surface of a WGM sensor (the plot indicates the microsphere transmittance vs. wavelength).

are to obtain the maximum amount of information from the smallest amount of sample, and to detect many binding events simultaneously.

The optical techniques used for sensing are based on phase changes (change in the index of refraction), amplitude changes (absorption) or frequency changes (fluorescence). The phase and amplitude changes represent a direct monitoring technique, whereas the frequency changes often need a marker (labeled system). The disadvantages of the labeled system (cost, expenditure, possibly reduced reactivity) are normally compensated by lower LOD, while in the case of direct monitoring the disadvantage lies in the ineffectiveness of detecting small molecular weights analytes and the sensitivity to nonspecific binding. Recently, however, the ability of detecting small absolute amounts of bound analyte, down to 0.25 fmol of streptavidin, via displacement of the resonance frequencies of the WG modes, was proved [105].

A spherical microcavity resonates when the guided light returns in phase coherently after every revolution, requiring an integer number of modes in one circumnavigation. The light outcoupled into the tapered fiber then shows a dip at the resonant wavelength in the spectral transmittance. A frequency shift of the resonances, when the radius and/or the refractive index of the sphere change, makes possible the utilization of the WGMs of microspheres to detect trace amounts of chemical and biological molecules. In other words, when the analyte aggregates at the surface, it interacts with the evanescent part of the WGM field inducing a change in the Q factor or a shift in the wavelength, as sketched in Fig. 19. The latter can be then quantitatively predicted using a perturbation theory [106]:

$$\Delta\lambda/\lambda = \alpha_{\rm ex}\,\sigma / \left[\varepsilon_0 \left(\nu_\sigma^2 - n_{\rm m}^2\right) a\right] \ , \qquad (36)$$

where $\alpha_{\rm ex}$ is the excess of polarizability and σ the surface density of molecules forming a layer. This equation is exact if the layer is considerably thinner than the evanescent field depth. Obviously, to observe the shift, $\Delta\lambda$ has to be comparable to, or larger than, the resonance bandwidth $\delta\lambda$.

Among the different optical sensor principles, none is generally superior but rather its convenience depends on the application. Most of the optical sensors are based on detection by the evanescent field at the transducer surfaces [107]. WGM sensors can be used for label-free [108, 109] and/or labeled detection [110, 111]. In the former case, as the analyte binds to the bioreceptor, the resonance shifts (the wavelength locations of the resonances depend on the size and refractive index of the WGM resonators); by measuring the shift, the amount of analyte bound can be quantified. In the latter case, the long photon lifetime enhances dramatically the absorption quantum efficiency of the fluorophores, resulting in an enhanced fluorescent emission.

A crucial step for producing effective biosensors is the surface functionalization, i.e. the chemical modification of the transducer's surface. Proteins adhere to any glass surface, rising the unwanted nonspecific effects. There are several ways of functionalizing the surface of a biosensor; among them, the most common ones are based on the silanization of the glass surface through covalent binding of the silane groups with the glass surface and the use of biotin and/or streptavidin layers. The silanization shows a reduced nonspecificity and enables a further functionalization with ligands or receptors, whereas the latter technique is based on a high affinity binding with streptavidin and biotinylated molecules. This crucial layer, however, has to be very thin, between 10 and 100 nm (below the evanescent field tail), and homogeneous in order to preserve the high quality of the transducer. As WGM sensors aim at ultralow detection of binding events (either biological or chemical) at the interface of the microcavity [110], the surface functionalization steps (outlined in Fig. 20) are very important. Indeed, the quality factor of the microresonator can be partially spoiled during the various steps of surface functionalization, as shown by the resonance measurements reported in Fig. 21.

A new trend in label-free methods is related to the use of fluorescent polystyrene microspheres, usually quantum-dot-embedded microspheres, either for exploiting the emitted fluorescence as a local broadband light source to couple the light into the microsphere [112] or to decrease the density of WGMs and tune their positions [113].

One of the first applications of microspherical resonators was in the area of gas sensing, where optical methods have been successfully employed for a long time [114]: a prototype system for atmospheric and acetylene trace-gas detection was demonstrated [115].

Rosenberger demonstrated first theoretically [116], and then experimentally [117] cavity-enhanced absorption sensing by measuring the changes in the fractional depth K (Eq. (33)) of the resonance dip in intensity transmittance through the coupler. In the case of weak analyte absorption, the change of K is proportional to the change in analyte absorption coefficient, in analogy with Beer's Law. An experimental effective absorption path length L_{eff} can be found by measuring K in the absence of analyte and in its presence ($K + \Delta K$). Using this method a 20-fold enhancement in relative sensitivity was obtained in comparison to the frequency-shift method.

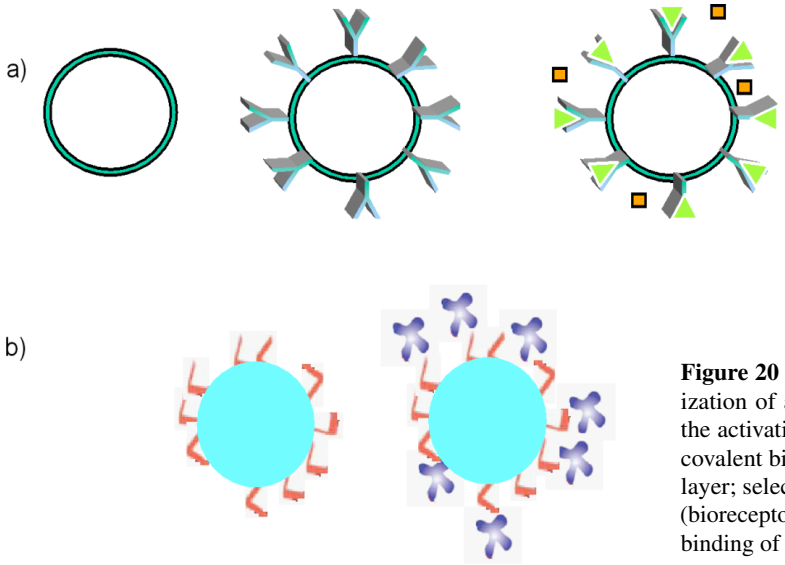

Figure 20 (online color at: www.lpr-journal.org) Functionalization of a WGM sensor: a) from left to right: deposition of the activation layer (*green color*) on the bare WGM resonator; covalent binding of the antibody (bioreceptor) to the activation layer; selective binding of the antigen (analyte) to the antibody (bioreceptor); b) deposition of a biotin layer (*red*), and selective binding of streptavidin (*blue*) to biotin.

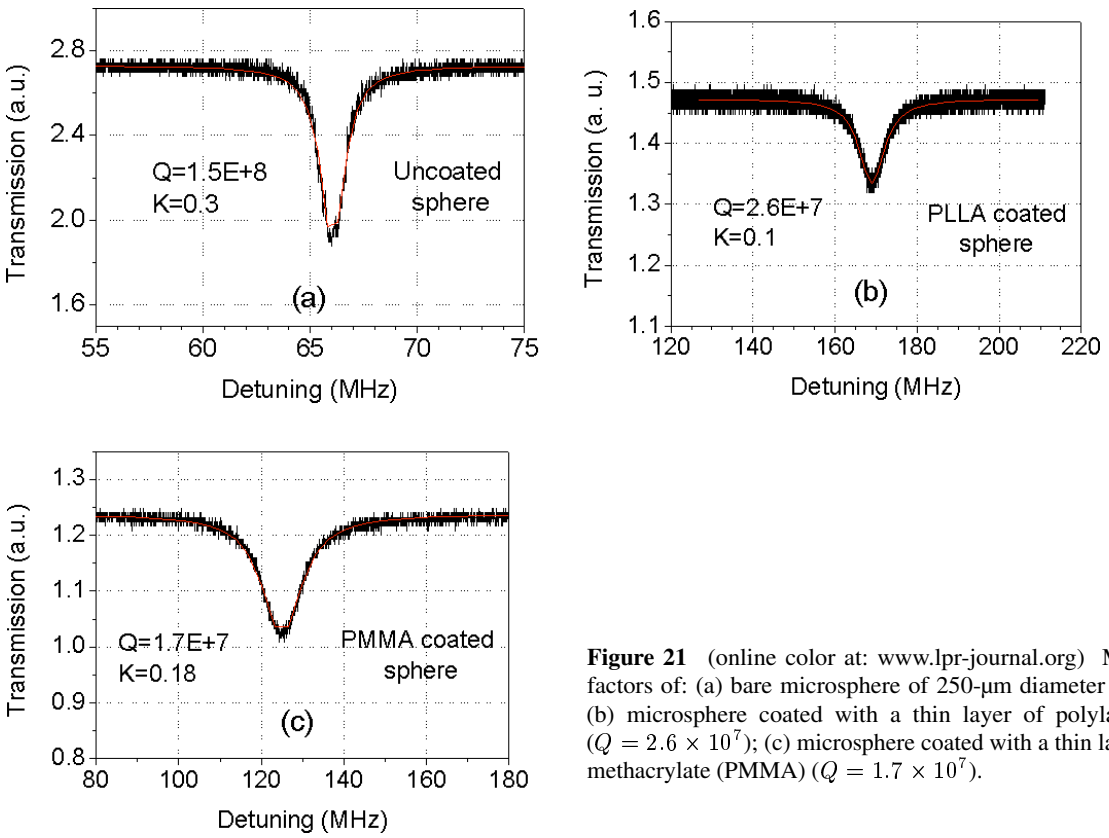

Figure 21 (online color at: www.lpr-journal.org) Measurement of Q factors of: (a) bare microsphere of 250-μm diameter ($Q = 1.5 \times 10^8$); (b) microsphere coated with a thin layer of polylactic acid (PLLA) ($Q = 2.6 \times 10^7$); (c) microsphere coated with a thin layer of Polymethylmethacrylate (PMMA) ($Q = 1.7 \times 10^7$).

More problems exist for sensing of (in) liquids: as a matter of fact, the Q factor of microspheres immersed in aqueous solutions is reduced to above 10^6 [108, 118]. Despite this, fused-silica microspheres have proved to be capable of mercury detection in water, with a detection limit of 50 ppb (w/w), which is comparable to results obtained using surface plasmon resonance [119]. Specific results concerning proteins like BSA [110], DNA [118] and protease [120], deposited on the surface of the microspheres, have shown that the LOD can be as low as 1–10 pg/mm^2. Vollmer et al. [118] also demonstrated that multiplexed DNA detection by using two microspheres was possible, and that a single nucleotide mismatch in an 11-mer[1] oligonucleotide could be discriminated.

[1] Mer indicates the repeating structural unit of any polymer. One mer is a monomer, two mers form a dimer, etc.

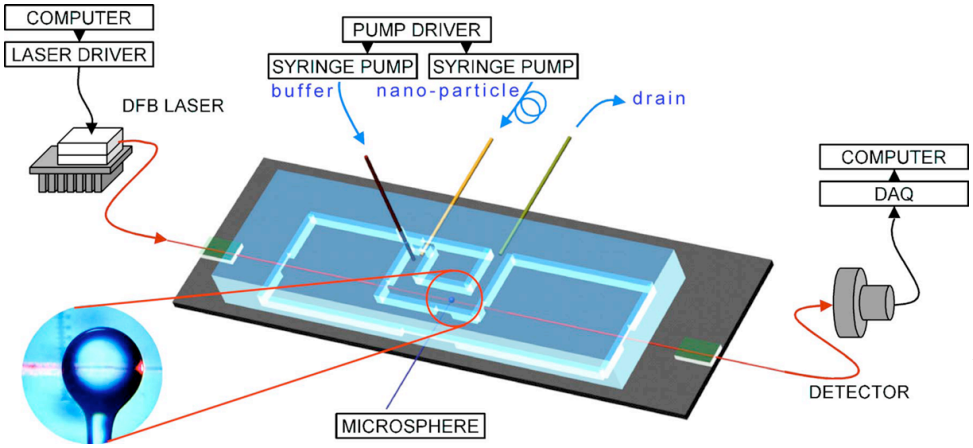

Figure 22 (online color at: www.lpr-journal.org) Microfluidic system incorporating a WGM sensor and a coupling fiber. (Reprinted with permission from [121]).

While the previous sensing applications had been implemented by simply measuring the dc component of the resonance wavelength shift signal, Arnold's group showed that the broadband "noise" on this signal provides physical information not available from its dc component [121]. They showed that stochastic effects associated with molecules undergoing Brownian motion near the resonator surface were responsible for the noise: the measurement of the signal autocorrelation function provides a first-order approximation for the nanoparticle size. They tested the method by realizing a microfluidic system, sketched in Fig. 22, and using polystyrene particles having a carboxylated surface and mean diameters of 37, 103, and 219 nm as simulants of bacterial virus. The results showed a good agreement for the smallest size and a progressive deviation for larger nanoparticle sizes, likely due to hydrodynamic effects near the phase boundary [121]. The same group was also demonstrating the detection of quite large particles, like rod-like bacteria, measuring down to 44 bacteria bound randomly to the surface [122]. In a recent comprehensive work on viral detection [123], they predicted LOD down to single virions, below the mass of HIV. Experimentally, they measured a surface coverage of MS2 (a virus icosahedral in shape like HIV) down to 0.2 pg/mm^2.

The use of TE and TM modes was also employed to determine protein orientation on a microsphere surface [124]. Protein adsorption was studied on different surface chemistries in different pH at different surface coverage: at low coverage, the TE/TM shift ratio allows one to estimate the polarizability anisotropy ratio of isolated molecules.

Conformations and orientations of molecules adsorbed on the surface of a microsphere can be also studied by employing the microsphere as an off-resonant spectroscopic tool [125].

Rhodamine 6G-doped polymer microspheres have also been proposed for sensing applications [126]; the analysis shows that active microcavities may possess an ultrahigh Q factor ($Q = 10^{10}$) and can therefore provide a very high sensitivity (up to $\Delta n_{eff} = 10^{-9}$ or an index change of the order of 10^{-7} in the surrounding water solution). In passive polymer microspheres, on the other hand, Q factors as high as 10^6 for spheres of 30 µm held by optical tweezers in aqueous solutions were measured [127]. The corresponding protein detection sensitivity was estimated around 0.25 pg/mm^2.

Two recent developments in this field have to do with the use of arrays or clusters of WGM resonators. The properties of an array of sixteen polymethyl methacrylate spherical microresonators placed on a microscope slide serving as an optical waveguide were studied for their use as a miniaturized high-resolution spectroscopic device [128]. A tunable narrowband laser source was coupled into the waveguide in order to generate an evanescent field and so to excite the microresonators. A particular intensity pattern in the array was thus generated, which depended sensitively on the wavelength: a resolution $\lambda/\Delta\lambda \sim 10^4$ was evaluated. Another proposal for a novel detection scheme for optical biosensing is based on the use of clusters of fluorescent microresonators; experimentally, polystyrene microspheres doped with Coumarin 6G dye were randomly deposited on a thin glass slide by drop coating from highly diluted suspension in order to form clusters of various sizes [129]. A microfluidic cell was then built around the slide. The clusters were exposed to a cw-HeCd laser operated at 442 nm, in order to excite WGMs (so overcoming the mechanical precision required for evanescent-field coupling), and the signal (from a single sphere or a cluster) was collected through an inverted microscope. This detection scheme permits the integration of a large number of detection sites within a single biosensor chip, with the advantage that each cluster can be read out properly even without knowledge of its precise position on the chip surface.

6.2. Mechanical and other sensors

The sensitivity of WGMs to external changes can be exploited in sensors of physical parameters too. An example is provided by an acceleration sensor, based on an architecture that, in order to make the coupling of light into WGMs easier and more efficient, combines stripline pedestal an-

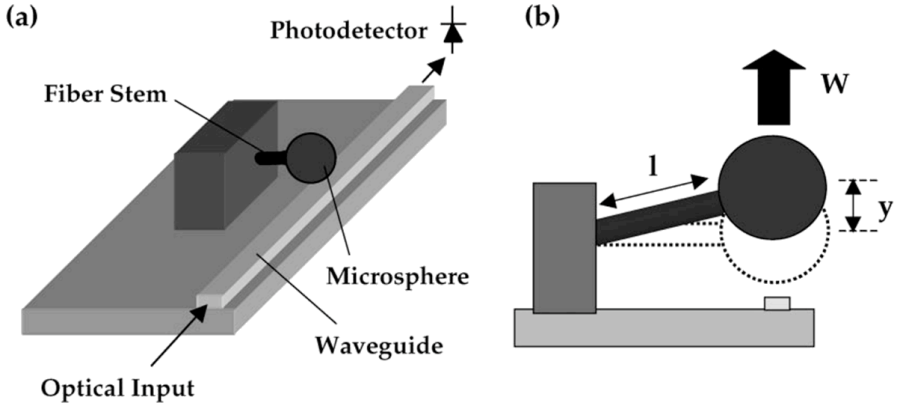

Figure 23 (a) Microsphere resonator, flexure stem, and SPARROW waveguide. (b) Cross-sectional view of the hybrid WGM as acceleration sensor. The microsphere displaces a distance y as a response of the load W. The stem length l and the diameter of the flexure are designed to satisfy system sensitivity and dynamic range requirements. (Reprinted with permission from [130]).

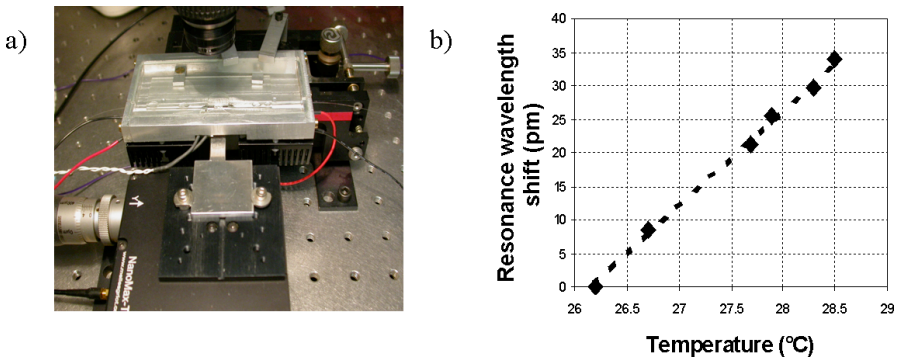

Figure 24 (online color at: www.lpr-journal.org) (a) Photograph of the thermostatic cell where the microsphere sensor is placed, (b) Resonance wavelength shift vs. temperature, for a microsphere of 350 µm diameter.

tiresonant reflecting optical waveguides (SPARROW) and a microsphere. The sensing method takes advantage of the variation of the coupling gap; the fiber stem that holds the microsphere (Fig. 23) functions as a flexure beam for the microresonator; when a force (provided by a piezoelectric shaker) is applied to the stem, the coupling gap changes (Fig. 23b) and the resonance properties change as well. Sensitivities better than 1 mg at 250 Hz bandwidth, with a noise floor of 100 µg were demonstrated [130].

Compressive forces and mechanical strains applied to a sphere may induce changes both in the shape and in the index of refraction of the sphere, again leading to a shift of WGMs. Some studies have discussed the use of applied mechanical strains to finely tune the resonance frequencies [131–133]. The induced shifts, however, may also be used to develop a micro-optical force sensor [134]. Experiments have been carried out on solid silica as well as solid and hollow PMMA microsphere resonators; a sensitivity as high as $d\lambda/dF$ = 7.664 nm/N was demonstrated with a 960-µm hollow PMMA sphere.

Similar considerations may be made for what refers to thermal effects. The control of temperature may be used to finely tune the resonance frequency [135–137], and, vice versa, WGM resonators can constitute sensitive temperature sensors [138]. We have been able to detect changes in the resonance wavelength of 14.2 ±0.4 pm/°C around 27 °C and 16.4 ±0.8 pm/°C around 54 °C [137]. Fig. 24 shows the experimental setup and the linear wavelength shift with temperature.

The idea of a miniature optical gyroscope based on a waveguide-coupled sequence of whispering-gallery mode microresonators was also discussed [139]. Even if practical problems exist (the coupling of many resonators to the single waveguide and achieving the same resonant frequency for all of them is not an easy task, and some individual trimming may be necessary), the composite system may allow for several orders of magnitude enhancement of sensitivity with respect to more conventional structures.

6.3. Filters

The unique spectral properties of WGM resonators, namely narrow linewidth, tunability and high stability, make them quite attractive for filtering applications. In optical telecommunications, the main task of the filters is to select channels in wavelength division multiplexing (WDM) schemes. An all-optical passive four-port system including a fused silica microsphere and two tapered fibers was proposed and demonstrated, to be used as a channel adding-dropping device [140]. The authors showed that channels can be selectively exchanged between two fibers by coupling to a whispering-gallery mode resonance in the microsphere. Finesse in excess of 11 150 was measured for the loaded whispering-gallery modes.

Microspheres were also used for polarization-insensitive optical channel dropping from an optical fiber half-coupler to a silicon photodetector in the M-band [141].

The dropped channels were observed both in the elastic scattering and the transmission spectra. The resonances had repetitive channel separations of 0.14 nm and linewidths of 0.06 nm. The filter dropped approximately 10% (0.5 dB) of the power at the resonance wavelength. The power detected by the photodiode was estimated to be 3.5% of the power in the fiber.

As already mentioned, the tunability of the WGM resonators can be achieved by several methods, in particular by mechanical trimming [131–133] and temperature tuning [135–137]. In both cases tuning ranges are relatively large, but the limit remains that a WGM resonator usually possesses small tuning speeds and low tuning accuracy.

WGM filters can be also used for laser stabilization. Rezac and Rosenberger [142] locked a microsphere to a frequency-scanning laser. The resonance frequency was modulated by axial compression of the microsphere, and phase-sensitive detection of the fiber-coupled optical throughput was used for locking. Compression modulation rates of up to 13 kHz were also achieved with this tuner.

Glass microsphere resonators can be also used as wavelength-selective feedback mirrors in fiber lasers; it has been demonstrated that a cw single-frequency fiber laser is possible, even with a long laser cavity, exploiting the narrow reflection bandwidth of such a microresonator [143]. Moreover, by modulating the reflectivity of a "microsphere mirror" in a fiber laser cavity, active Q switching may be achieved [144]. The laser cavity consisted of an Er-doped fiber, a fiber Bragg grating reflector at one end, and a microsphere reflector coupled through a fiber taper at the other end. By changing the gap between the microsphere and the fiber taper, the reflectivity of the microsphere is modulated, and giant pulses with a peak power > 100 W and duration ~ 160 ns have been obtained at a low pump power (~ 3 mW) threshold [144].

6.4. Microlasers

Miniature lasers are one of the most obvious applications of WGM resonators, and the very high quality factor of these resonators leads to a reduced threshold of lasing. The most common active material is glass, usually doped with luminescent elements, like rare-earth ions. Microspherical lasers based on crystalline materials [15], on the one hand, and on polymers and organic molecules [145, 146], on the other hand, have been demonstrated as well.

In one of the early papers, Sandoghdar et al. [92] reported the realization of a whispering-gallery-mode laser based on neodymium-doped silica microspheres. They analyzed the behavior of a typical microsphere with 56 µm diameter, made from a fiber with a core of 20 µm diameter containing about 0.2 wt% Nd, and a Q of 2×10^8. The microlaser threshold was measured by varying the incident pump power (from a laser diode at 807 nm) and monitoring the intensity of one of the longitudinal modes, using a monochromator as a filter; one of the lowest observed thresholds corresponded to an absorbed pump power of 200 nW [92]. Neodymium doping was also used for CW lasing in fluoride microspheres, fabricated by melting and abrupt cooling, according to the process already described in Sect. 3.1 [55]. By excitation at 800 nm, emission was observed corresponding to both $^4F_{3/2}$–$^4I_{11/2}$ ($\lambda = 1051$ nm) and $^4F_{3/2}$–$^4I_{13/2}$ ($\lambda = 1334$ nm) transitions. The corresponding threshold powers for a 170-µm diameter microsphere were 5 and 60 mW, respectively.

A microsphere made of highly doped erbium:ytterbium phosphate glass was used to generate light at 1.5 µm by Vahala's group [94]. The authors obtained a low laser threshold at pump power of 60 µW and a fiber-coupled output power as high as 3 µW with single-mode operation. A bisphere laser system consisting of two microspheres attached to a single fiber taper was also demonstrated.

In our group [147], we produced microspheres from different type of glasses: three experimental modified-silica glasses, doped with 0.2, 0.5, and 1.5 at.% of Er^{3+} (Baccarat Glass, labeled as B02, B05, and B15, respectively), and two commercial phosphate glasses, i.e. a sodium-alumino-phosphate glass (Schott IOG1) that contains 1.5 wt% of Er_2O_3 and 3 wt% of Yb_2O_3 and a potassium-barium-alumino phosphate glass (Schott IOG2) which contains 2 wt% of Er_2O_3 and 3 wt% of Yb_2O_3. The refractive indices at 632.8 nm of the three modified-silica glasses are equal to 1.5604, 1.5607, and 1.5871, respectively, while those of the phosphate glasses are 1.5270 and 1.5220, respectively.

Pieces of each bulk glass were first ground, and microspheres were then fabricated using a plasma torch, as mentioned in Sect. 3.1. The experimental setup for laser characterization of Er^{3+}-doped microspheres is sketched in Fig. 25. Among the different pumping wavelengths that can be used to excite Er^{3+} ions in oxide glasses (810, 980 and 1480 nm) we chose 1480 nm so that phase and mode-matching condition between the fiber coupler and the microsphere can be better fulfilled at both the pump and the laser wavelengths. We used standard fiber-optic components, either spliced or connected with APC connectors. The system consists of a fiber pigtailed tunable pump laser diode, an isolator that prevents feedback into the laser diode, an attenuator, and a 1.48/1.55- µm multiplexer that is finally connected to the tapered fiber coupler. The multiplexer also allows us to simply use a half-taper as the coupling device: in fact the counter-propagating fluorescence or laser signal from the sphere can be collected by the same coupling fiber and directed to an optical spectrum analyzer (OSA) through the 1.55-µm port of the WDM. When, instead, a biconical tapered fiber is used as a coupler, we can collect either the counterpropagating signal or the copropagating one. In order to control the position of the microsphere relative to the taper, the fiber stem (on which the microsphere is mounted) is placed on a translation stage with piezoelectric actuators and a positioning resolution of 20 nm.

The different WGMs emission spectra from a B05 glass microsphere with a diameter of 85 µm are shown in Fig. 26, where the curve (x 1000) indicates the fluorescence spectrum with a series of peaks that can be assigned to several families of WGMs [148]. Laser oscillation was ob-

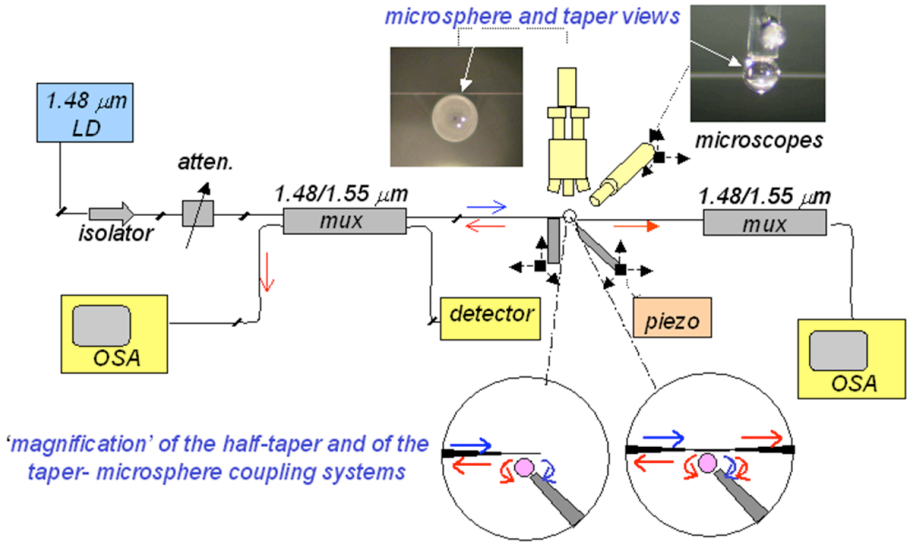

Figure 25 (online color at: www.lpr-journal.org) Sketch of the experimental setup for coupling light in the Er^{3+}-doped microspheres and for the characterization of their WGMs emission spectra.

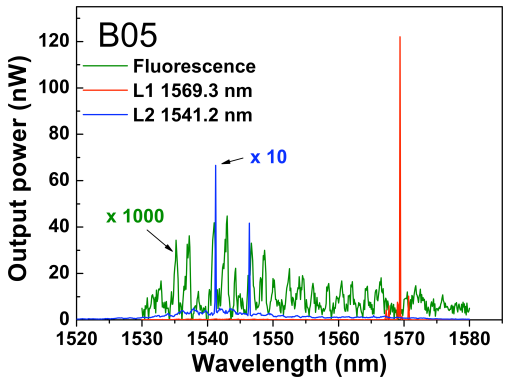

Figure 26 (online color at: www.lpr-journal.org) WGMs emission spectra from a 85-μm microsphere in B05 glass: fluorescence spectrum (measured with a wavelength bandwidth of 0.1 nm) and laser spectra corresponding to the maximum (L1) and minimum (L2) wavelength peak values.

tained when increasing the pump intensity above a minimum threshold of 2.5 mW. By varying the contact position of the tip of the half-taper fiber coupler relative to the sphere and increasing the pump power, the lasing spectrum moved towards WGMs of shorter wavelength. The tuning range is about 30 nm wide, from a maximum wavelength of 1569.3 nm (red peak) to a minimum (blue peak) of 1541.2 nm. A similar shift was observed in an Er^{3+}-doped tellurite microlaser [54]: as the actual wavelength of the lasing mode is determined by both the gain of the material and the WGM of the microsphere, one observes a discrete rather than continuous shift. A continuous shift, permitting a fine tuning of the laser wavelength, is possible only in a short interval (of the order of nm) when one WGM is fixed and the pump power is also slightly increased. The same group achieved a maximum output power of 0.12 mW at 1561 nm when pumping at 1480 nm a microsphere of tellurite glass doped with 0.5 wt% Er_2O_3 [148].

Similar results have been obtained for microspheres made in IOG2 phosphate glass (in a 70-μm diameter microsphere the lasing wavelength interval was ∼ 40 nm) and in IOG1 phosphate glass (70 μm sphere; lasing wavelength interval ∼ 34 nm).

In the last decade new approaches for fabricating low-threshold microspherical lasers have been reported as well. Yang and Vahala [149] coated silica microspheres with active layers by means of sol-gel technique; both continuous-wave (cw) and pulsed operation were possible by control of the coating thickness. CW laser operation (threshold 28 μW) was observed with a coating thickness of roughly 1 μm, whereas pulsed-laser operation was possible for coatings of about 5 μm in thickness; the single-mode laser produced an output power of 10 μW. Shopova et al. [150] demonstrated laser action in a silica microsphere coated with HgTe quantum dots (QD). The laser wavelengths ranged from 1240 to 1780 nm depending on the composition and size of the QDs. For microspheres of diameter about 950 μm the threshold was about 200 nW and the maximum output power ∼ 40 μW, whereas for smaller microspheres the threshold was about 9.4 μW and the achieved output power ∼ 80 μW.

Cha et al. [151] showed lasing action in hollow semiconductor microspheres with core-shell nanocrystals. With the help of water-soluble block peptides the hollow microspheres were cooperatively assembled with walls composed of an inner layer of core-shell CdSe/CdS QD surrounded by an outer thinner layer of silica nanoparticles. The authors observed a laser line at 542 nm for 2.8-μm diameter microspheres and at 538 nm for 3.3-μm diameter microspheres. The measured threshold was 0.8 mJ for a Q-switched ND:YAG pump laser (10 ns, 10 Hz) at 355 nm.

Rakovich et al. [152] studied the optical properties of a melamine formaldehyde latex microsphere coated with CdTe quantum dots, but despite observing sharp Lorentzian peaks in the photoluminescence spectra, there was no clear evidence of lasing. The curves do not show a threshold

Table 2 Summary of the results obtained in microspherical glass lasers.

$\lambda_{\text{emission}}$ [μm]	P_{th}	Peak power	R[μm]	*Coupling system*	*Material (glass)*
1.06–1.09	200 nW	10–150 pW	25–50	Prism	Nd-doped silica [92]
1.051 and 1.334	5–60 mW	not available	130–140	Free-Space	Nd-doped fluoride [55]
1.5	60 μW	3 μW	50–100	Taper	Er:Yb phosphate glass [94]
540 nm	30 μW	not available	120	Prism	Er^{3+}-doped ZBLAN [95]
1.565	86 μW	200 μW	40	Taper	silica (Raman Laser) [97]
1.56	600 μW	140 nW	53	Half-taper/ Taper	Er^{3+}-doped ZBLAN [153]
1.569	2.5 mW	120 nW	85	Half-taper/ Taper	Er^{3+}-doped Baccarat [147]
1.568	not available	18 μW	70	Half-taper/ Taper	Schott IOG2 phosphate [147]
1.61	1.4 mW	124.5 μW	16	Taper	Er^{3+}-doped tellurite [148]
1.535	28 μW	10 μW	50–80	Taper	Er^{3+} doped coated silica [149]
1.24–1.78	200 nW	40 μW	950	Taper	HgTe QD coated silica [150]
542 nm 538 nm	0.86 mJ (pulsed)	Not available	2.8 3.3	Microscope objective	double layer CdSe-CdS QD/ silica [151]

dependence and an enhanced scattering at the laser line without QD was also observed.

A summary of the results obtained in microspherical lasers made in different glass materials is provided in Table 2, where P_{th} indicates the threshold power, usually measured at the input of the coupling system, and R is the radius of the microsphere.

Microspheres can play an important role in developing compact and low-threshold laser sources operating in the visible region as well, which are in high demand in several domains of commercial interest. Indeed, except for the blue, which can be covered by using the recently developed GaN semiconductor laser diodes, no reliable and wavelength well-adapted laser sources are yet commercially available between 525 and 630 nm in the green to orange range. An interesting demonstrator, based on an upconversion process, was proposed for a green laser using a 120- μm diameter microsphere of Er^{3+}-doped ZBLAN glass [95]. Lasing occurs at room temperature around 540 nm, by relaxation from the $^4S_{3/2}$ state of the Er^{3+} ion, using a 801-nm diode laser pump. The lasing threshold was only 30 μW of absorbed power although a possible photodarkening effect was suggested [95]. Anyway, upconversion-based spherical microlasers appear to be suitable candidates to develop reliable and wavelength well-adapted laser sources.

7. Conclusions and outlook

Spherical microresonators, and especially glass microspheres, have been discussed here in terms of fundamental properties, fabrication protocols, light-injection configuration, diagnostic techniques, and applications. This field represents a hot topic nowadays, and the research covers several significant scientific and technological areas, from fundamental physics to sophisticated sensing applications, passing through materials science and photonics.

The unique properties of spherical microresonators, their very high quality factor Q, the possibility of tailoring the glass composition and of functionalizing the spheres by appropriate passive or active coatings, together offer us a very sensitive tool. With this tool one can study and give experimental demonstration of impressive physical effects of cavity quantum electrodynamics, such as the modification of the homogeneous broadening of rare-earth optical transitions, and nonlinear effects such as stimulated Raman scattering, four-wave parametric oscillation, or very low threshold laser action.

On the application side, there is an increasing interest toward advanced sensing, and this review reports several examples of biochemical sensing both for label-free and labeled detection. On the other hand, the optical properties of these microresonators depend on the applied compressive forces and mechanical strain; some recent applications of microspheres as force sensors are reported, and it is easy to foresee that spherical microresonators can play an important role for monitoring fatigue phenomena in civil structures where a local detection is required.

Many practical issues are still to be faced to realize these possibilities, and, indeed, so far we have to deal with laboratory prototypes only. The main problem is the lack of integration. Ideally, multiplexed WGMR should provide rapid information on both chemical composition of real samples, i.e. blood or serum, and toxins or disease-marker screening. For fabricating a lab-on-a-chip, state-of-the-art photolithographic fabrication techniques could provide microfluidic cells. Microcavities combined with nanoplasmonics can increase the local optical field at the surface and open up the possibility of surface-enhanced Raman spectroscopy of the molecules of interest. Conformational changes were recently proved and this approach can be extended to measurements of protein folding, so that we could expect that WGM sensors will be used for high sensitivity early detection of Alzheimer and/or Huntington diseases.

Microlaser sources still remain one of the more exciting and versatile outcomes of spherical microresonators, and the examples presented here are far from exhaustive. Although the attention has mainly been focused on the 1.5-μm region, looking at the research trends in this field it is reasonable to expect important outcomes also in visible compact laser sources; they could have a considerable impact on optical data storage and medicine. The optimization of the fabrication protocol of active microspheres is crucial to achieve a high quality factor, in particular for materials characterized by low cutoff vibrational energy.

One avenue to explore could be that of developing nanocomposite spheres with core-shell configuration; the sol-gel shell can be loaded by nanocrystals with low phonon energy, activated by rare-earth ions. Some encouraging results have already been obtained, also by our group.

Another line of research that has been proposed but not pursued enough is related to the use of active microspheres as biosensors. By functionalizing them properly, one might have the laser source and the sensing device in a single resonator.

Quantum applications, not reviewed in this paper, can profit from the improvement of fabrication techniques and obtain additional gains in chip QED. High Purcell factors may lead to single-photon sources. In technological applications such as filtering, add and drop devices will improve the control and reproducibility of filtering properties of the device. Nonlinear effects triggered by the enhanced field in a microsphere could span the emission down to the ultraviolet and operate continuously.

As a summary, we can conclude that glass-based spherical microresonators are a very handy tool to study and apply important physical effects. The major present challenge is how to pass from the laboratory to the market, by developing rugged devices that undoubtedly would have large interest for application in sensing, biomedical diagnostics, metrology and telecommunications.

Acknowledgements We wish to thank a number of colleagues who have been collaborating with us for many years: Simone Berneschi, Massimo Brenci, Ilaria Cacciari, Roberto Calzolai, Franco Cosi (IFAC CNR, Florence), Cristina Armellini, Andrea Chiappini, S. N. B. Bhaktha (IFN CNR, Trento), Maurizio Mattarelli, Maurizio Montagna, Enrico Moser, Cristiana Tosello (Physics Dept., University of Trento). Part of this work was supported by the EFONGA European Coordination Action, NAoMI PAT project, and Centro Fermi.

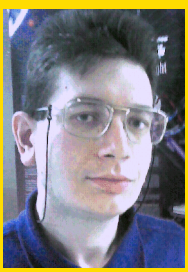

Alessandro Chiasera received the Ph. D. degree in physics from the Trento University, Trento, Italy, in 2003. He is currently a Researcher with the National Research Council of Italy, Institute for Photonics and Nanotechnologies, Povo-Trento, Italy. Since 2000, his principal activity has been in the investigation of the properties and the development of materials and structures for photonics applications. This research activity is related to the activities of the CSMFO Group. He has 161 scientific articles in international journals and 169 communications at national and international congresses; he is involved in several national and international projects concerning glass photonics.

Yannick Dumeige graduated from the École Supérieure d'Optique, Orsay, France, in 1999 and received the Ph. D. degree from the University of Paris XI, Orsay, in 2002. He spent 2002 with the Laboratoire de Photonique Quantique et Moléculaire, Cachan, France. Since 2003, he has been with the École Nationale Supérieure des Sciences Appliquées et de Technologies, University of Rennes 1, Lannion, France, as an Associate Professor. His current research interest is integrated nonlinear optics.

Patrice Féron received the Ph. D. degree from the University of Paris XI, Orsay, France, in 1988. He is a Professor with the École Nationale Supérieure des Sciences Appliquées et de Technologies, University of Rennes 1, Lannion, France, which is an engineering school. His current research interests are mainly in the areas of microcavities and whispering-gallery-mode resonators for laser and all-optical function applications.

Maurizio Ferrari received the Ph. D. degree in physics from Trento University, Trento, Italy, in 1981. Until 1998, he worked as a Researcher with the Laboratoire de Physico-Chimie des Matériaux Luminescents, Lyon, France, and in 1998 he moved to Trento as a Researcher with the National Research Council of Italy (CNR). He is currently a Senior Researcher with the Institute for Photonics and Nanotechnologies, CNR, where he is the Head of the CSMFO Group and is responsible for research activities in photonics-materials, structures, and diagnostics. He is co-author of more than 300 publications in international journals, of several book chapters and he is involved in numerous national and international projects concerning glass photonics.

Yoann Jestin received the M. S. and Ph.D degrees from the University of Rennes and University of Le Mans, France, in 1999 and 2002, respectively. He has been awarded a temporary research position at the PhLAM laboratory in the university of Lille, France. Since 2004 he received a post-doctoral training at the institute of Photonic and Nanotechnologies of the CNR, Italy. His current research interests include, but are not restricted to, application of whispering-gallery resonators in photonics, optical waveguide amplifiers, photonic crystals. Dr. Jestin is a member of the Italian Society of Optics and Photonics (SIOF).

Gualtiero Nunzi Conti is a researcher at the "Nello Carrara" Institute of Applied Physics (IFAC-CNR). He previously worked at the Centro Fermi in Rome, at the Optical Sciences Center of the University of Arizona, and at NP Photonics, Inc., in Tucson, AZ, USA. He holds a Ph. D. in Electronic Engineering and a *laurea* degree in Physics. His main interests are in the area of fiber, glass integrated optics, and micro-optics for communications and sensing. He has published more than 30 papers in ISI journals, about 50 in international conference proceedings and holds one US patent.

Stefano Pelli holds a *laurea* in Physics and a Ph. D. in Non Destructive Testing from the Università di Firenze. He is a researcher at the "Nello Carrara" Institute of Applied Physics (IFAC-CNR). His interests are focused in the fields of integrated and fibre optics, glasses for optoelectronics applications, microresonators. He is co-author of more than 60 papers in ISI Journals and about 90 in conference proceedings. Dr. Pelli is the 2009–2010 President of SIOF.

Silvia Soria holds an M. Sc. and a Ph. D. degree in Physics from the University of Barcelona in Spain, and a *laurea* in Physics from the Università di Firenze, Italy. She has worked at Laser Laboratorium Goettingen e.V., in Germany, and at ICFO-Institute of Photonics Science in Barcelona, Spain where she was a Ramon y Cajal researcher and the PI of several projects. Currently she is a researcher of the Centro Studi e Ricerche "E. Fermi" and an associated researcher at IFAC- CNR. Her areas of research include lasers, nonlinear optics, soft matter and optical biosensing. She has authored over 27 papers and presented her results in many international congresses.

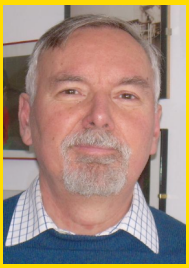

Giancarlo C. Righini received the *laurea* (doctor in Physics) degree from the University of Firenze in 1967. After having been Research Fellow at the University, since 1972 he is in the staff of the National Research Council of Italy (CNR). From 2006 to 2009 he has been Director of the CNR national Department on Materials and Devices; he is now research director at IFAC - CNR and contract professor of optoelectronics at the University of Firenze. His research interests concern guided-wave optics, glasses for optoelectronics, grating structures, THz photonics. He has published over 300 papers (half of them in peer-reviewed journals), and is coauthor of 6 international Patents. Very recently he has co-edited a book on *Introduction to Optoelectronic Sensors*. He is member of the Board of the European Optical Society and member of the Editorial Board of various International Journals. He is Member of OSA, Fellow of EOS, Fellow of SPIE and Emeritus Member of SIOF.

References

[1] A. N. Oraevsky, Gaussian Beams and Optical Resonators, Proc. of the Lebedev Physics Institute (Nova Science Publishers, Hauppauge, NY, USA, 1995).

[2] N. Hodgson and H. Weber, Optical Resonators: Fundamentals, Advanced Concepts and Applications (Springer-Verlag Telos, Santa Clara, CA, USA, 1997).

[3] R. Kossowsky, M. Jelinek, and J. Novák, eds., Optical Resonators – Science and Engineering, NATO ASI Series (Kluwer Academic Publishing, Norwell, MA, USA, 1998).

[4] J. Weiner and K. C. Dee, Light-Matter Interaction: Fundamentals and Applications (Wiley-Interscience, Weinheim, 2003).

[5] D. R. Hall and P. E. Jackson, The Physics and Technology of Laser Resonators (Taylor & Francis, London, 1989).

[6] V. P. Bykov and O. O. Silichev, Laser Resonators (Cambridge International Science Publishers, Cambridge, 1995).

[7] A. V. Kudryashov and H. Weber, Laser Resonators: Novel Design and Development (SPIE Press, Bellingham, WA, USA, 1999).

[8] N. Hodgson and H. Weber, Laser Resonators and Beam Propagation, 2nd ed. (Springer, New York, 2005).

[9] H. Yokoyama and K. Ujihara, eds., Spontaneous Emission and Laser Oscillation in Microcavities (CRC Press, Boca Raton, 1995).

[10] Lord Rayleigh, Philos. Mag. **20**, 1001 (1910); Sci. Pap. **5**, 617 (1912).
[11] C. V. Raman and G. A. Sutherland, Proc. R. Soc. Lond. A **100**, 424 (1921); Nature **108**, 42 (1921).
[12] A. Ashkin and J. M. Dziedzic, Appl. Opt. **20**, 1803 (1981).
[13] C. C. Lam, P. T. Leung, and K. Young, J. Opt. Soc. Am. B **9**, 1585 (1992).
[14] R. D. Richtmyer, J. Appl. Phys. **10**, 319 (1939).
[15] C. G. B. Garrett, W. Kaiser, and W. L. Bond, Phys. Rev. **124**, 1807 (1961).
[16] K. J. Vahala, Nature **424**, 839 (2003).
[17] J. Heebner, R. Grover, and T. Ibrahim, Optical Microresonators (Springer, London, 2007).
[18] A. Matsko, ed., Practical Applications of Microresonators in Optics and Photonics (Taylor and Francis, Boca Raton, FL, USA, 2009).
[19] J. M. Gerard, B. Sermage, B. Gayral, B. Legrand, E. Costard, and V. Thierry-Mieg, Phys. Rev. Lett. **81,** 1110 (1998).
[20] B. E. Little, S. T. Chu, H. A. Haus, J. Foresi, and J. P. Laine, J. Lightwave Technol. **15**, 998 (1997).
[21] P. P. Absil, Microring resonators for wavelength division multiplexing and integrated photonics applications, Ph. D. dissertation, University of Maryland, College Park (2000).
[22] Y. Kokubun, in: Photonics Based on Wavelength Integration and Manipulation, IPAP Books 2 (IPAP, Tokyo, 2005), pp. 303–316.
[23] D. G. Rabus, Integrated Ring Resonators: The Compendium (Springer, Berlin, 2007).
[24] J. Sarma and K. A. Shore, IEE Proc. J. (Optoelectron.) **132**, 325 (1985).
[25] S. L. McCall, A. F. J. Levi, R. E. Slusher, S. J. Pearton, and R. A. Logan, Appl. Phys. Lett. **60**, 289 (1992).
[26] K. Djordjev, S.-J. Choi, S.-J. Choi, and P. D. Dapkus, IEEE Photon. Technol. Lett. **14**, 828 (2002).
[27] M. Borselli, K. Srinivasan, P. E. Barclay, and O. Painter, Appl. Phys. Lett. **85**, 3693 (2004).
[28] D. K. Armani, T. J. Kippenberg, S. M. Spillane, and K. J. Vahala, Nature **421**, 925 (2003).
[29] D. K. Armani, B. K. Min, A. L. Martin, and K. J. Vahala, Appl. Phys. Lett. **85**, 5439 (2004).
[30] T. J. Kippenberg, S. M. Spillane, and K. J. Vahala, Phys. Rev. Lett. **93**, 083904 (2004).
[31] M. Hossein-Zadeh and K. J. Vahala, Opt. Express **15**, 166 (2007).
[32] K. Srinivasan, P. Barclay, O. Painter, J. Chen, C. Cho, and C. Gmachl, Appl. Phys. Lett. **83**, 1915 (2003).
[33] P.-T. Lee, T.-W. Lu, F.-M. Tsai, and T.-C. Lu, Appl. Phys. Lett. **89**, 231111 (2006).
[34] P.-T. Lee, T.-W. Lu, J.-H. Fan, and F.-M. Tsai, Appl. Phys. Lett. **90**, 151125 (2007).
[35] H.-M. Tzeng, K. F. Wall, M. B. Long, and R. K. Chang, Opt. Lett. **9**, 273 (1984).
[36] H.-M. Tzeng, K. F. Wall, M. B. Long, and R. K. Chang, Opt. Lett. **9**, 499 (1984).
[37] H. B. Lin, A. L. Huston, and A. J. Campillo, Opt. Lett. **11**, 614 (1986).
[38] A. Biswas, H. Latifi, R. L. Armstrong, and R. G. Pinnick, Opt. Lett. **14**, 214 (1989).
[39] S. D. Druger, S. Arnold, and L. M. Folan, J. Chem. Phys. **87**, 2649 (1987).
[40] H. B. Lin, J. D. Eversole, and A. J. Campillo, J. Opt. Soc. Am. B **9**, 43 (1992).
[41] J. Stratton, Electromagnétisme (Masson, Paris, 1960).
[42] J. Jackson, Classical Electrodynamics, 3rd edn. (John Wiley and Sons, New York, 1999).
[43] C. C. Lam, P. T. Leung, and K. Young, J. Opt. Soc. Am. B **9**(9), 1585–1592 (1992).
[44] M. Abramowitz and I. Stegun, in: Handbook of Mathematical Functions (Dover Publications, New York, 1970), pp. 366–367, 446.
[45] H. M. Nussenzveig, Diffraction Effects in Semi-classical Scattering (Cambridge University Press, Cambridge, 1992).
[46] P. Féron, Ann. Fond. Louis Broglie **29**, 297 (2004).
[47] M. L. Gorodetsky and A. E. Fomin, IEEE J. Sel. Top. Quantum Electron. **12**, 33 (2006).
[48] M. L. Gorodetsky, A. A. Savchenkov, and V. S. Ilchenko, Opt. Lett. **21**, 453 (1996).
[49] A. A. Savchenkov, A. B. Matsko, M. Mohageg, and L. Maleki, Opt. Lett. **32**, 497 (2007).
[50] Y. Dumeige, S. Trebaol, L. Ghisa, T. K. N. Nguyên, H. Tavernier, and P. Féron, J. Opt. Soc. Am. B **25**, 2073 (2008).
[51] F. Treussart, Etude expérimentale de l'effet Laser dans des microsphères de silice dopées avec des ions néodyme, Ph. D. thesis, Université Paris VI (1997).
[52] P. Tien, Appl. Opt. **10**, 2395 (1970).
[53] K. H. Guenter and P. G. Wierer, Proc. SPIE **401**, 266 (1983).
[54] X. Peng, F. Song, S. Jiang, N. Peyghambarian, M. Kuwata-Gonokami, and L. Xu, Appl. Phys. Lett. **82**, 1497 (2003)
[55] K. Miura, K. Tanaka, and K. Hirao, J. Non-Cryst. Solids **213**, 276 (1997).
[56] N. Kitamura, M. Makihara, M. Hamai, T. Sato, I. Mogi, S. Awaji, K. Watanabe, and M. Motokawa, Jpn. J. Appl. Phys. **39**, L324 (2000).
[57] N. Kitamura, M. Makihara, T. Sato, M. Hamai, I. Mogi, S. Awaji, K. Watanabe, and M. Motokawa, J. Non-Cryst. Solids **293–295**, 624 (2001).
[58] G. Nunzi Conti, A. Chiasera, L. Ghisa, S. Berneschi, M. Brenci, Y. Dumeige, S. Pelli, S. Sebastiani, P. Feron, M. Ferrari, and G. C. Righini, J. Non-Cryst. Solids **352**, 2360 (2006).
[59] L. Yang and K. J. Vahala, Opt. Lett. **28**, 592 (2003).
[60] K. Naoyuki, M. Masaki, M. Iwao, A. Satoshi, W. Kazuo, and M. Mitsuhiro, Jpn. J. Appl. Phys. 1 **44**, 7546 (2005).
[61] Y. Jestin, C. Armellini, A. Chiappini, A. Chiasera, Y. Dumeige, M. Ferrari, P. Féron, L. Ghisa, G. Nunzi Conti, S. Trebaol, and G. C. Righini, Proc. SPIE **6890**, 689008-1 (2008).
[62] W. Stober, A. Fink, and E. Bohn, J. Colloid Interf. Sci. **26**, 62 (1968).
[63] M. J. A. de Dood, B. Berkhout, C. M. van Kats, A. Polman, and A. van Blaaderen, Chem. Mater. **14**, 2849 (2002).
[64] G. C. Righini, C. Armellini, A. Chiasera, Y. Jestin, M. Ferrari, A. Chiappini, M. Montagna, C. Arfuso Duverger, P. Féron, S. Berneschi, M. Brenci, G. Nunzi Conti, S. Pelli, C. Gonçalves, and R. M. Almeida, Glass Technology – Eur. J. Glass Sci. Technol. A **48**, 200 (2007).
[65] K. Yamaguchi, T. Niimi, M. Haraguchi, T. Okamoto, and M. Fukui, Jpn. J. Appl. Phys. **45**, 6750 (2006).
[66] J. C. Knight, G. Cheung, F. Jacques, and T. A. Birks, Opt. Lett. **22**, 1129 (1997).

[67] J.-P. Laine, B. E. Little, and H. A. Haus, IEEE Phot. Technol. Lett. **11**, 1429 (1999).
[68] M. Cai and K. Vahala, Opt. Lett. **26**, 884 (2001).
[69] Y. Panitchob, G. Senthil Murugan, M. N. Zervas, P. Horak, S. Berneschi, S. Pelli, G. Nunzi Conti, and J. S. Wilkinson, Opt. Express **16**, 11066 (2008).
[70] M. L. Gorodetsky and V. S. Ilchenko, Opt. Commun. **113**, 133 (1994).
[71] S. Ilchenko, X. S. Yao, and L. Maleki, Opt. Lett. **24**, 723 (1999).
[72] S. M. Spillane, T. J. Kippenberg, O. J. Painter, and K. J. Vahala, Phys. Rev. Lett. **91**, 043902 (2003).
[73] G. Griffel, S. Arnold, D. Taskent, and A. Serpenguzel, Opt. Lett. **21**, 695 (1996).
[74] M. L. Gorodetsky and V. S. Ilchenko, J. Opt. Soc. Am. B **16**, 147 (1999).
[75] G. C. Righini, M. Brenci, A. Chiasera, P. Feron, M. Ferrari, G. Nunzi Conti, and S. Pelli, Proc. SPIE **6029**, 602903 (2005).
[76] M. C. Cai, O. Painter, and K. J. Vahala, Phys. Rev. Lett. **85**, 74 (2000).
[77] J. E. Heebner, V. Wong, A. Schweinsberg, R. W. Boyd, and D. J. Jackson, IEEE J. Quantum Electron. **40**, 726 (2004).
[78] B. E. Little, J.-P. Laine, and H. A. Haus, J. Lightwave Technol. **17**, 704 (1999).
[79] H. J. Schmitt and H. Zimmer, IEEE Trans. Microw. Theory Tech. **MTT-14**, 206 (1966).
[80] Z. K. Ioannidis, P. M. Radmore, and I. P. Giles, Opt. Lett. **13**, 422 (1988).
[81] J. Morville, D. Romanini, M. Chenevier, and A. Kachanov, Appl. Opt. **41**, 6980 (2002).
[82] G. Ying, H. Ma, and Z. Jin, Appl. Opt. **46**, 4890 (2007).
[83] Z. Li, R. G. T. Bennett, and G. E. Stedman, Opt. Commun. **86**, 51 (1991).
[84] J. Poirson, F. Bretenaker, M. Vallet, and A. Le Floch, J. Opt. Soc. Am. B **14**, 2811 (1997).
[85] M. J. Lawrence, B. Willke, M. E. Husman, E. K. Gustafson, and R. L. Byer, J. Opt. Soc. Am. B **16**, 523 (1999).
[86] L. Matone, M. Barsuglia, F. Bondu, F. Cavalier, H. Heitmann, and N. Man, Phys. Lett. A **271**, 314 (2000).
[87] A. A. Savchenkov, A. B. Matsko, V. S. Ilchenko, and L. Maleki, Opt. Express **15**, 6768 (2007).
[88] T. Kippenberg, Nonlinear Optics in Ultra-high-Q Whispering-Gallery Optical Micro-cavities, Ph. D. Thesis, California Institute of Technology, Pasadena (2004), Chap. 3.
[89] P. McMillan, Am. Mineral. **69**, 622 (1984).
[90] D. R. Vij, Luminescence of Solids (Plenum Press, New York, 1998).
[91] G. C. Righini and M. Ferrari, Riv. Nuovo Cimento **28**, 1 (2005)
[92] V. Sandoghdar, F. Treussart, J. Hare, V. Lefevre-Seguin, J. M. Raimond, and S. Haroche, Phys. Rev. A **54**, R1777 (1996).
[93] F. Lissillour, P. Féron, N. Dubreuil, P. Dupriez, M. Poulain, and G. Stéphan, Electron. Lett. **36**, 1382 (2000)
[94] M. Cai, O. Painter, K. J. Vahala, and P. C. Sercel, Opt. Lett. **25,** 1430 (2000).
[95] W. von Klitzing, E. Jahier, R. Long, F. Lissillour, V. Lefèvre-Seguin, J. Hare, J.-M. Raimond, and S. Haroche, J. Opt. B **2**, 204 (2000).
[96] K. Sasagawa, K. Kusawake, J. Ohta, and M. Nunoshita, Electron. Lett. **38**, 1355 (2002).
[97] S. M. Spillane, T. J. Kippenberg, and K. J. Vahala, Nature **415**, 621 (2002).
[98] H. Fujiwara and K. Sasaki, Jpn. J. Appl. Phys. 2 **41**, L46 (2002).
[99] I. S. Grudinin and L. Maleki, J. Opt. Soc. Am. B **25**, 594 (2008).
[100] C. Arnaud, M. Boustimi, M. Brenci, P. Féron, M. Ferrari, G. Nunzi Conti, S. Pelli, and G. Righini, Proc. SPIE **5622**, 315 (2004).
[101] C. Duverger, M. Montagna, R. Rolli, S. Ronchin, L. Zampedri, M. Rossi, S. Pelli, G. C. Righini, A. Monteil, C. Armellini, and M. Ferrari, J. Non-Cryst. Solids **280**, 261 (2001).
[102] P. Flubacher, A. J. Leadbetter, J. A. Morrison, and B. P. Stoicheff, J. Phys. Chem. Solids **12**, 53 (1959)
[103] J. C. Phillips, Solid State Phys. **37**, 93 (1982)
[104] D. R. Theâvenot, K. Toth, R. A. Durst, and G. S. Wilson, Pure Appl. Chem. **71**, 2333 (1999).
[105] Y. Lin, V. Ilchenko, J. Nadeau, and L. Maleki, Proc. SPIE **6452**, 64520U (2007).
[106] I. Teraoka, S. Arnold, and F. Vollmer, J. Opt. Soc. Am. B **20**, 1937 (2003).
[107] X. Fan, I. M. White, S. I. Shopova, H. Zhu, J. D. Suter, and Y. Sun, Anal. Chim. Acta **620**, 8 (2008).
[108] F. Vollmer, D. Braun, A. Libchaber, M. Khoshsima, I. Teraoka, and S. Arnold, Appl. Phys. Lett. **80**, 4057 (2002).
[109] N. M. Hanumegowda, C. J. Stica, B. C. Patel, I. M. White, and X. Fan, Appl. Phys. Lett. **87**, 201107 (2005).
[110] J. L. Nadeau, V. S. Ilchenko, D. Kossakovski, G. H. Bearman, and L. Maleki, Proc. SPIE **4629**, 172 (2002).
[111] S. C. Hill, P. Nachmann, S. Arnold, J. M. Ramsey, and M. D. Barnes, J. Opt. Soc. Am. B **16**, 1868 (1999).
[112] S. Pang, R. E. Beckham, and K. E. Meissner, Appl. Phys. Lett. **92**, 221108 (2008).
[113] D. E. Gomez, I. Pastoriza-Santos, and P. Mulvaney, Small **2**, 238 (2005).
[114] I. Cacciari and G. C. Righini, Optical gas sensing, in: Solid State Gas Sensing, edited by E. Comini, G. Faglia, G. Sberveglieri (Springer, New York, 2009).
[115] A. T. Rosenberger and J. P. Rezac, Proc. SPIE **3930**, 186 (2000).
[116] A. T. Rosenberger, Opt. Express **15**, 12959 (2007).
[117] S. L. Westcott, J. Zhang, R. K. Shelton, N. M. K. Bruce, S. Gupta, S. L. Keen, J. W. Tillman, L. B. Wald, B. N. Strecker, A. T. Rosenberger, R. R. Davidson, W. Chen, K. G. Donovan, and J. V. Hryniewicz, Rev. Sci. Instrum. **79**, 033106 (2008).
[118] F. Vollmer, S. Arnold, D. Braun, I. Teraoka, and A. Libchaber, Biophys. J. **85**, 1974 (2003).
[119] N. M. Hanumegowda, I. M. White, and X. Fan, Sens. Actuators B, Chem. (Switzerland) **120**, 207 (2006).
[120] N. Hanumegowda, I. M. White, H. Oveys, and X. Fan, Sens. Lett. **3**, 315 (2005).
[121] D. Keng, S. R. MacAnanama, I. Teraoka, and S. Arnold, Appl. Phys. Lett. **91**, 103902 (2007).
[122] H. C. Ren, F. Vollmer, S. Arnold, and A. Libchaber, Opt. Express **15**, 17410 (2007).

[123] S. Arnold, R. Ramjit, D. Keng, V. Kolchenko, and I. Teraoka, Faraday Discuss. **137**, 65 (2008).
[124] M. Noto, D. Keng, I. Teraoka, and S. Arnold, Biophys. J. **92**, 4466 (2007).
[125] J. Topolancik and F. Vollmer, Biophys. J. **92**, 2223 (2007).
[126] J. Yang and L. J. Guo, IEEE J. Sel. Top. Quantum Electron. **12**, 143 (2006).
[127] J. Lutti, W. Langbein, and P. Borri, Appl. Phys. Lett. **91**, 141116 (2007).
[128] G. Schweiger, R. Nett, and T. Weigel, Opt. Lett. **32**, 2644 (2007).
[129] A. François and M. Himmelhaus, Appl. Phys. Lett. **92**, 141107 (2008).
[130] J. P. Laine, C. Tapalian, B. Little, and H. Haus, Sens. Actuators A, Phys. (Switzerland) **93**, 1 (2001).
[131] V. S. Ilchenko, P. S. Volikov, V. L. Velichansky, F. Treussart, V. Lefevre-Seguin, J.-M. Raimond, and S. Haroche, Opt. Commun. **145**, 86 (1998).
[132] W. von Klitzing, R. Long, V. S. Ilchenko, J. Hare, and V. Lefevre-Seguin, Opt. Lett. **26**, 166 (2001).
[133] T. Ioppolo and M. V. Ötügen, J. Opt. Soc. Am. B **24**, 2721 (2007).
[134] T. Ioppolo, M. Kozhevnikov, V. Stepaniuk, M. V. Ötügen, and V. Sheverev, Appl. Opt. **47**, 3009 (2008).
[135] D. W. Vernooy, A. Furusawa, N. P. Georgiades, V. S. Ilchenko, and H. J. Kimble, Phys. Rev. A **57** R2293 (1998).
[136] H. C. Tapalian, J. P. Laine, and P. A. Lane, IEEE Photon. Technol. Lett. **14**, 1118 (2002).
[137] M. Brenci, R. Calzolai, F. Cosi, G. Nunzi Conti, S. Pelli, and G. C. Righini, Proc. SPIE **6158**, 61580S (2006).
[138] G. Guan, S. Arnold, and M. V. Ötügen, AIAA J. **44**, 2385 (2006).
[139] A. B. Matsko, A. A. Savchenkov, V. S. Ilchenko, and L. Maleki, Opt. Commun. **233**, 107 (2004).
[140] M. Cai, G. Hunziker, and K. Vahala, IEEE Photon. Technol. Lett. **11**, 686 (1999).
[141] T. Bilici, S. Isci, A. Kurt, and A. Serpenguzel, IEEE Photon. Technol. Lett. **16**, 476 (2004).
[142] J. P. Rezac and A. T. Rosenberger, Opt. Express **8**, 605 (2001).
[143] K. Kieu and M. Mansuripur, Opt. Lett. **32**, 244 (2007).
[144] K. Kieu and M. Mansuripur, Opt. Lett. **31**, 3568 (2006).
[145] M. Kuwata-Gonokami and K. Takeda, Opt. Mater. **9**, 12 (1998).
[146] Y. Hara, K. Takeda, and M. Kuwata-Gonokami, IEE QELS Postconference Digest (2003).
[147] G. Nunzi Conti, S. Soria, S. Berneschi, M. Brenci, F. Cosi, S. Pelli, C. Armellini, A. Chiappini, A. Chiasera, Y. Jestin, M. Ferrari, E. Moser, L. Ghisa, S. Trebaol, Y. Dumeige, P. Féron, and G. C. Righini, Adv. Sci. Technol. **55**, 46 (2008).
[148] X. Peng, F. Song, M. Kuwata-Gonokami, S. Jiang, and N. Peyghambariam, Opt. Eng. **44**, 034202 (2005).
[149] L. Yang and K. J. Vahala, Opt. Lett. **28**, 592 (2003).
[150] S. I. Shopova, G. Farca, A. T. Rosenberger, W. M. S. Wickramanayake, and N. A. Kotov, Appl. Phys. Lett. **85**, 6101 (2004).
[151] J. N. Cha, M. H. Bartl, M. S. Wong, A. Popitsch, T. J. Deming, and G. D. Stucky, Nano Lett. **3**, 907 (2003).
[152] Y. P. Rakovich, L. Yang, E. M. McCabe, J. F. Donegan, T. Perova, A. Moore, N. Gaponik, and A. Rogach, Semicond. Sci. Technol. **18**, 914 (2003).
[153] F. Lissillour, D. Messager, G. M. Stéphan, and P. Féron, Opt. Lett. **26**, 1051 (2001).